Digital Comprehensive Summaries of Uppsala Dissertations
from the Faculty of Pharmacy 410

Pharmacokinetic Mechanisms in the Development and Prevention of Chemotherapy-Induced Peripheral Neuropathy

Milda Girdenytė

ACTA UNIVERSITATIS
UPSALIENSIS
2026

UPPSALA
UNIVERSITET

Dissertation presented at Uppsala University to be publicly examined in Room IV, Biskopsgatan 3, Uppsala, Friday, 6 November 2026 at 09:15 for the degree of Doctor of Philosophy (Faculty of Pharmacy). The examination will be conducted in English. Faculty examiner: Professor Tore Bjerregaard Stage (University of Southern Denmark, Department of Public Health).

Abstract

Girdenytė, M. 2026. Pharmacokinetic Mechanisms in the Development and Prevention of Chemotherapy-Induced Peripheral Neuropathy. *Digital Comprehensive Summaries of Uppsala Dissertations from the Faculty of Pharmacy* 410. 72 pp. Uppsala: Acta Universitatis Upsaliensis. ISBN 978-91-513-2960-4.

Chemotherapy-induced peripheral neuropathy (CIPN) is a major dose-limiting adverse effect of anticancer microtubule-targeting agents (MTAs). However, the pharmacologically active unbound exposure of MTAs at CIPN-relevant sites, including peripheral and central nervous system tissues and skeletal muscle, and its relationship to neurotoxicity and biomarkers remain incompletely characterized. The overall aim of this thesis was to investigate MTAs distribution and intra- and extracellular exposure at CIPN-relevant sites using preclinical models and integrating these findings with pharmacokinetic-pharmacodynamic (PKPD) modelling and biomarker evaluation to improve understanding and monitoring of CIPN in patients.

Particular emphasis was placed on paclitaxel-induced peripheral neuropathy (PIPN), with focus on drug formulation, translational pharmacokinetics, and serum neurofilament light chain (sNfL) as a biomarker of axonal injury. Albumin-bound and micellar paclitaxel formulations showed greater unbound distribution across endothelial barriers at CIPN-relevant sites, expressed as the unbound tissue-to-plasma concentration ratio (Kp,uu,tissue), than paclitaxel formulated with Cremophor EL. Results provide a plausible mechanistic explanation for the higher incidence of CIPN with non-Cremophor EL formulations. Based on PIPN site pharmacokinetic data, a semi-mechanistic PKPD model was developed linking sNfL kinetics to intracellular paclitaxel-tubulin binding in dorsal root ganglia, peripheral nerves, and brain. The framework was translated to humans, where sNfL dynamics were related to the Total Neuropathy Score-clinical version in breast cancer patients. sNfL showed moderate predictive performance for CIPN, highlighting the multifactorial nature of PIPN.

The thesis was subsequently extended to cabazitaxel, docetaxel, vinorelbine, and eribulin to investigate whether differences in CIPN prevalence could be related to MTA distribution at CIPN-relevant sites. Despite differences in the time required to reach steady-state, governed by tubulin abundance and transporter-mediated distribution across endothelial and parenchymal barriers, all MTAs showed a similar distribution pattern, with greater distribution into PNS than CNS tissues. Thus, dissimilarities in clinical unbound plasma exposure, rather than in tissue distribution patterns, may be important determinants of intracellular exposure and neurotoxicity.

Together, the translational framework developed in this thesis links drug exposure, intracellular target engagement, and sNfL dynamics from preclinical to clinical settings. It provides a rationale for PK-informed CIPN assessment and for the development of novel MTAs with reduced neurotoxicity.

Keywords: chemotherapy-induced peripheral neuropathy, blood-dorsal root ganglion barrier, blood-nerve barrier, blood-brain barrier, taxanes, Vinca alkaloids, drug distribution

Milda Girdenytė, Department of Pharmacy, Box 580, Uppsala University, SE-75123 Uppsala, Sweden.

© Milda Girdenytė 2026

ISSN 1651-6192
ISBN 978-91-513-2960-4
URN urn:nbn:se:uu:diva-599159 (http://urn.kb.se/resolve?urn=urn:nbn:se:uu:diva-599159)

Šeimai, draugams ir mokytojams —
Už bures, pilnas vėjo, ir už pasaulį, prasidedantį nuo mažų atradimų.

For my family, friends, and mentors —
for wind-filled sails and for a world that begins with small discoveries.

List of Papers

This thesis is based on the following papers, which are referred to in the text by their Roman numerals.

I. **Girdenytė M**, Hu Y, Ginosyan A, Hammarlund-Udenaes M, Loryan I. (2024) Formulation-dependent differences in paclitaxel distribution to anatomical sites relevant to chemotherapy-induced peripheral neuropathy. *Front. Pharmacol*. Doi: 10.3389/fphar.2024.1486686

II. Ibrahim, EIK*, **Girdenytė M***, Hu Y, Mannelli LDC, Balayssac D, Busserolles J, Theil D, Roussignol G, Perrault O, Le Berre N, Chanut F, Slaoui M, Loryan I[§], Friberg LE[§]. (2026) Evaluation of sNfL as a Biomarker for Paclitaxel-Induced Peripheral Neurotoxicity Through an Integrated PKPD Model. *Pharm Res*. Doi.org/10.1007/s11095-026-04053-z

III. Ibrahim, EIK, **Girdenytė M**, Velasco R, Bruna J, Argyriou AA, Kalofonos HP, Loryan I[§], Friberg LE[§]. Leveraging PKPD Modelling and Simulation to Characterize sNfL Dynamics and Predict Paclitaxel-Induced Peripheral Neurotoxicity in Patients. *Clin Pharmacol Ther*. *Submitted*

IV. **Girdenytė M.**, Ginosyan A, Jadhari R, Hammarlund-Udenaes M, Loryan I. Eribulin exhibits a reduced distribution pattern across CNS and PNS barriers compared to Cremophor EL/ethanol solubilized paclitaxel. *In manuscript*

V. **Girdenytė M.**, Ginosyan A, Jadhari R, Hammarlund-Udenaes M, Loryan I. The role of tissue distribution of microtubule-targeting agents in the development of chemotherapy-induced peripheral neurotoxicity. *In manuscript*

* Shared first authorship

[§] Shared last authorship

Reprints were made with permission from the respective publishers.

Related publications

Hu Y, **Girdenytė M**, Roest L, Liukkonen I, Siskou M, Bällgren F, Hammarlund-Udenaes M, Loryan I. (2024) Analysis of the contributing role of drug transport across biological barriers in the development and treatment of chemotherapy-induced peripheral neuropathy. *Fluids Barriers CNS*. Doi: 10.1186/s12987-024-00519-7

Contents

Introduction 13
CIPN as a clinical burden 14
Risk of CIPN development 14
Manifestation of CIPN and its evaluation 15
MTAs and CIPN development 16
Role of biological barriers in CIPN development 18
CIPN sites 18
Barriers controlling distribution of MTAs to CIPN sites 19
MTA transport to CIPN sites 20
Methods to investigate CIPN site pharmacokinetics 21
Approaches to investigate tissue-to-plasma ratios 22
Blood-based monitoring biomarkers for CIPN 25
Mathematical PKPD-biomarker modelling: focus on paclitaxel 26

Aims of the thesis 28

Material and methods 29
Drug selection 29
Animals 29
Evaluation of the unbound partition coefficient to CIPN sites 30
Total tissue distribution 30
Intra-tissue distribution 31
Plasma and tissue binding 32
Assessment of steady-state attainment in CIPN sites 33
NfL kinetics after bolus paclitaxel administration 34
Bioanalysis 35
UPLC-MS/MS 35
Automated Immunoassay System 35
Statistical analysis 36
Mathematical modeling 36
Data used for modelling purposes 36
Model building workflow 37

Results and Discussion 39
From paclitaxel distribution to NfL-guided CIPN prediction 39
Formulation and premedication impact on MTA distribution 39
NfL kinetics after paclitaxel administration 40

Paclitaxel PK and NfL kinetics model....42
CIPN prediction via paclitaxel PK-NfL-TNSc model....45
The contributing role of tissues to the elevation of sNfL....46
Distribution to CIPN sites and tubulin engagement of MTAs....46
Time needed to reach steady-state in tissues among MTAs....46
The extent of unbound MTAs' distribution to CIPN sites....47
Estimation of relative TO....49

Conclusions....52

Future perspectives....55

Popular science summary....57

Acknowledgements....59

References....62

Abbreviations

ADC	Antibody-drug conjugate
aECF	Artificial extracellular fluid
A_{tissue}	Amount of the drug in the tissue
AUC	Area under the concentration-time curve
BBB	Blood-brain barrier
BDB	Blood-dorsal root ganglion barrier
BI	Bounded integer
BNB	Blood-nerve barrier
Br	Brain
BSA	Body surface area
BSCB	Blood-spinal cord barrier
BSMI	Blood-skeletal muscle interface
C_{donor}	Drug concentration at the donor side
CI	Confidence interval
CIPN	Chemotherapy-induced peripheral neuropathy (neurotoxicity)
CL	Systemic clearance
$CL_{in,tissue}$	Net influx clearance of unbound drug across a barrier
cLogP	Calculated octanol/water partition coefficient
$CL_{out,tissue}$	Net efflux clearance of unbound drug across a barrier
CMA	Combinatory Mapping Approach
CNS	Central nervous system
CRCI	Chemotherapy-related cognitive impairment
$C_{receiver}$	Drug concentration at the receiver side
CrEL	Cremophor EL
CSF	Cerebrospinal fluid
$C_{through}$	Plasma concentration of the drug measured at the end of a dosing interval
CTCAE	Common terminology criteria for adverse events
$C_{tot,plasma,ss}$	Total plasma concentration at steady-state
$C_{u,buffer}$	Unbound drug concentration in the buffer
$C_{u,ICF,tissue}$	Unbound intracellular tissue concentrations
$C_{u,plasma}$	Unbound drug concentration in plasma
DRG	Dorsal root ganglion

ELISA	Enzyme-linked immunosorbent assay
FOCEI	First-order conditional estimation method with interaction
$f_{u,plasma}$	The fraction of unbound drug in the plasma
$f_{u,tissue}$	The fraction of unbound drug in the tissue
IDP	Individual dynamic prediction
IV	Intravenous
K_d	Equilibrium dissociation constant
$k_{el,tissue}$	Tissue elimination constant
$K_{p,tissue}$	Total tissue-to-plasma ratio
$K_{p,uu,cell}$	Unbound intracellular-to-extracellular concentration ratio
$K_{p,uu,tissue}$	Unbound tissue-to-plasma concentration ratio
MTA	Microtubule-targeting agent
nab	Albumin-bound
NfL	Neurofilament light chain
NLME	Non-linear mixed-effects
OAT	Organic anion transporter
OATP	Organic anion-transporting polypeptide
OFV	Objective function value
P	Drug permeability
PBS	Phosphate-buffered saline
PD	Pharmacodynamics
P-gp	P-glycoprotein
PIPN	Paclitaxel-induced peripheral neuropathy (neurotoxicity)
PK	Pharmacokinetics
PN	Peripheral nerve
PNS	Peripheral nervous system
popPK	Population PK
PsN	Perl-speaks-NONMEM
Q1W	Weekly
Q3W	Every-3-weeks
ROC	Receiver operating characteristic
RSE	Relative standard error
SA	Surface area
SAEM	Stochastic approximation expectation maximization
SC	Spinal cord
SIR	Sampling importance resampling
SM	Skeletal muscle
SN	Sciatic nerve
sNfL	Serum neurofilament light chain
TNS	Total neuropathy scale

TNSc	Total neuropathy scale-clinical score
TO	Tubulin occupancy
TRITC	Tetramethylrhodamine isothiocyanate
VPC	Visual predictive check
V_{ss}	Volume of distribution at steady-state
$V_{u,tissue}$	Unbound volume of distribution in the tissue
V_i	Residual volume of aECF surrounding the tissue

Introduction

Cancer is a leading cause of death and reduced quality of life worldwide, with the number of new diagnoses growing each year (1). To alleviate the burden and prolong the survival of cancer patients, medical and pharmacological interventions have been developed throughout the years. This initially included surgical treatments and radiotherapy, with the introduction of chemotherapy in the 1940s, and a few decades later, a breakthrough in pharmacological treatment using new modalities, like targeted therapy and antibody-drug conjugates (ADCs) (2, 3). Even though the goal of decreasing cancer progression and increasing survival rates in many cases has been achieved, the management of cancer treatment side effects has become a recurring challenge (4). These unwanted effects differ by treatment, with the most common ones including haematological toxicities, hair loss, nausea, cutaneous reactions, immune-related adverse events, and neurotoxicity (4). The latter remains an often dose-limiting long-term side effect of small molecules and novel therapies (4, 5). Furthermore, there is a lack of effective preventive or curative treatments due to a lack of understanding of the pharmacokinetic (PK) and pharmacodynamic (PD) aspects of the development of chemotherapy-induced peripheral neuropathy (CIPN) (5), which hinders the advancement in the search for novel CIPN prevention and treatment strategies.

In recent decades, research on the development mechanisms of CIPN has been increasing (6). Chemotherapeutic classes such as platinum agents, proteasome inhibitors, and most often, microtubule-targeting agents (MTAs) like paclitaxel and *Vinca* alkaloids, have been extensively studied for their molecular, cellular, and systemic mechanisms of action related to the progression of neurotoxicity (6). Based on current scientific knowledge, there is a gap in understanding the link between MTAs' systemic and CIPN-relevant tissue pharmacokinetics, describing the time course of drug concentrations in blood and tissues, including their distribution to the tissues of toxicity. Thus, this thesis focuses on the extent of distribution of selected MTAs to CIPN sites and explores neurofilament light chain (NfL) as a potential monitoring biomarker for paclitaxel-induced CIPN. Together, these findings can improve understanding of how drug exposure contributes to CIPN and support the development of better prevention, monitoring, and treatment strategies for cancer patients.

CIPN as a clinical burden

CIPN is a prominent adverse event, characterized as a symmetrical, sensory-predominant neuropathy and described as chemotherapy-induced damage of peripheral nerves (5). This term emphasizes that the neuronal dysfunction happens outside the brain and spinal cord (5). Although "neuropathy" is widely used in the context of CIPN, the term alone generally refers to a nerve disorder or injury. "Neurotoxicity", in contrast, describes the toxic effects of a drug or other substance on the nervous system. Furthermore, from a clinical perspective, the term "polyneuropathy" better denotes the clinical pattern of CIPN, involving multiple nerves across the nervous system (7). In this thesis, the terms "neuropathy" and "neurotoxicity" are used interchangeably, and CIPN refers to an adverse event of chemotherapy, in which sensory, motor, or other nerves may be affected and lead to numbness, pain, and muscle weakness.

Risk of CIPN development

In general, a varying degree of CIPN is associated with the treatment of several anticancer agents. A meta-analysis, which included some of the most frequently used anticancer drugs, like paclitaxel, vincristine, oxaliplatin, cisplatin, bortezomib, and thalidomide, showed that within two months after initial chemotherapy treatment, the mean of 68.1 % (95% confidence interval (CI): 57.7–78.4 %) of patients start to experience CIPN-related symptoms (8). Another analysis showed that MTAs were associated with a greatly increased risk of CIPN compared to other drugs, with a hazard ratio of 9.04 (9). Due to chemotherapy's harmful effect on the nervous system, patients' recovery can be partial, with the mean of 30.0 % (95% CI: 6.4–53.5 %) of patients having persistent CIPN symptoms at 6 months and longer (8). For example, paclitaxel-induced peripheral neuropathy (PIPN) persisted for over 3 years in 41% of breast cancer patients (10).

The risk of CIPN development is suggested to be linked with older age, alcohol abuse, smoking, inherited neuropathy, and other comorbidities, like diabetes mellitus (Fig. 1) (11). The risk of CIPN is associated with the selected treatment and higher single-dose or overall cumulative systemic chemotherapy plasma exposure (5, 12). In the case of dosing regimen, a randomized clinical trial comparing 80 mg/m^2 weekly infusion for 1 hour (Q1W) and 175 mg/m^2 every-3-weeks infusion for 3 hours (Q3W) treatment of paclitaxel in metastatic breast cancer patients showed that a weekly dosing regimen improves treatment efficacy, but also increases the prevalence of severe neuropathy (13). However, a later meta-analysis showed a trend of lower neuropathy risk among patients receiving a weekly paclitaxel dosing regimen (14).

Nevertheless, the increase in CIPN severity in patients leads to dose reduction or treatment cessation to mitigate the development of adverse effects (15), which lowers treatment efficacy for cancer patients.

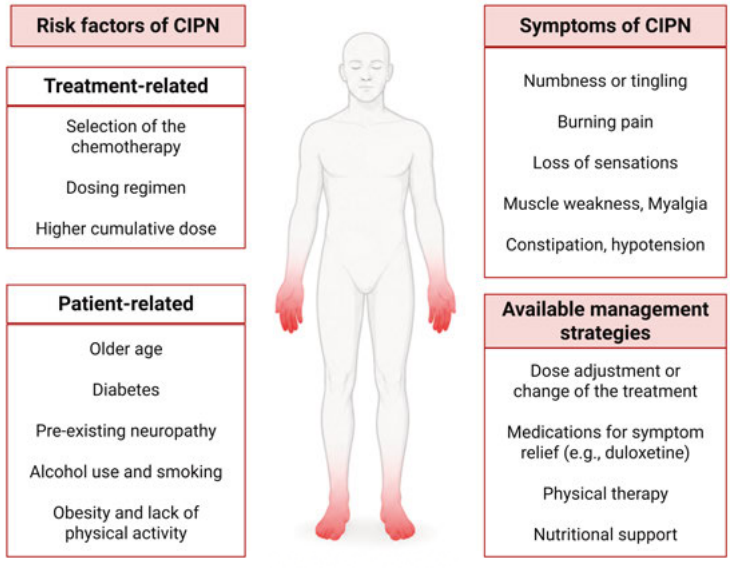

Figure 1. Overview of risk factors, clinical symptoms, and available management strategies for chemotherapy-induced peripheral neuropathy (CIPN).

Manifestation of CIPN and its evaluation

From the clinical perspective, the development of CIPN leads to specific symptoms, which decrease the patients' long-term well-being. CIPN has been described as a sensory axonal neuropathy, with occasional development of motor or autonomic neuropathy symptoms, depending on the administered drug (5, 16). The symptoms are known to have a "stocking-and-glove" distribution, due to the sensory dysfunction and altered pain perception in the body extremities (17). CIPN manifests mainly as paresthesia or hypoesthesia, developing into neuropathic pain. In some cases, patients experience myalgia and autonomic dysfunction, like constipation and hypotension (Fig. 1) (5, 16). In addition to CIPN, patients may experience symptoms of chemotherapy-related cognitive impairment (CRCI) or chemo brain (18). This includes patients with CIPN reporting greater insomnia severity, anxiety, and depression (19). The overall burden of CIPN on patients is increased due to the lack of effective treatment for CIPN, with few options focusing on lowering pain sensation but not treating CIPN itself (Fig. 1) (5).

The severity of overall CIPN, including the mentioned symptoms, can be determined using various approaches, such as clinician- and patient-reported outcome measurements, including Common Terminology Criteria for Adverse Events (CTCAE) and Total Neuropathy Scale (TNS) (20). CTCAE is based on clinician-assessed sensory and motor symptoms and their functional impact (21). TNS is a combination of different examinations, including patient-reported symptoms, clinical examination, neurophysiological and quantitative sensory testing, each one graded from 0 (normal) to 4 (severe abnormality) (22). To increase the feasibility of TNS, a clinical version (TNSc) was developed by excluding nerve-conduction studies and quantitative sensory tests. Thus, TNSc is often used to assess the severity and changes in CIPN-related symptoms (23). Due to the subjective nature of these scoring systems, trained personnel may evaluate CIPN severity differently, challenging an even assessment and management of CIPN development across multiple cancer centers. CIPN-related blood biomarkers can be a useful strategy to increase the objectivity in CIPN assessment. However, no biomarker has been validated for the monitoring of CIPN in clinic (5).

MTAs and CIPN development

MTAs target microtubules, hollow structures made from tubulin, a 110 kDa heterodimer of different types of α and β tubulin subunits (24). Microtubules have an important role in mitosis, therefore, MTAs are extensively used in cancer treatment to disrupt mitotic spindle formation and lead cancer cells to cell death (24). In high concentrations, MTAs either increase or decrease microtubule mass in the cell via induction of microtubule polymerization or depolymerization, as shown in cell culture assays (25), and suppress microtubule dynamics (26). Thus, MTAs are classified as microtubule stabilizer and destabilizer agents (Table 1). One of several useful measures of drug-target interaction is tubulin occupancy (TO), defined as the fraction of total tubulin bound by the drug. In a fibrosarcoma cell model, a TO of at least 10% was required to observe taxane-induced loss of microtubule dynamics (27).

Although this mechanism of action is effective for killing rapidly dividing cells, when MTAs reach healthy cells, including neurons, they can affect the structural role of microtubules. In the case of CIPN development, MTAs-induced disruption of axonal transport and mitochondrial function in neurons is suggested to be one of several mechanisms contributing to the neurotoxicity of these drugs (28). However, the required relative TO for microtubule stabilizers and destabilizers remains unknown to induce CIPN development.

Table 1. Summary of clinically used MTA with a focus on common dosing regimens in clinical settings, tubulin binding site, and CIPN prevalence presented as min – max determined in different patient populations. Abbreviations: Q3W – every-3-weeks, Q1W – weekly, IV - intravenous

	Tubulin binding site	Common dosing regimen used in clinical settings (infusion time)$	CIPN prevalence Grade 1-4#	Severe CIPN prevalence Grade 3-4#	Reference to CIPN prevalence report
Stabilizers					
Paclitaxel	Taxanes/ epothilones domain (29)	175 mg/m² (3 h) 100 mg/m² (1 h)	57–83%	7–33%	(30)
Cabazitaxel		20 mg/m² (1 h)	14% ¤	1% ¤	(31)
Docetaxel		75 mg/m² (1 h)	46–58%	1–3%	(32)
Ixabepilone		40 mg/m² (3 h)	63% ¤	14% ¤	(33)
Destabilizers					
Vincristine	*Vinca* domain (29)	1.4 mg/m² (5 min)	3–100%*	4-14%	(34, 35)
Vinblastine		6 mg/m² (3 min)	26% ¤	0% ¤	(36)
Vinorelbine		25 mg/m² (10 min)	22% ¤	2% ¤	(37)
Vindesine		3 mg/m² (10 min)	47% ¤	8.8% ¤	(38)
Vinflunine		320 mg/m² (20 min)	17% ¤	0% ¤	(39)
Eribulin		1.4 mg/m² (5 min)	32% ¤	5.4% ¤	(40)

$ Dosing regimens are reported in the Summary of Product Characteristics of each drug. # CIPN was graded according to the CTCAE. *The incidence rate varied widely depending on ethnicity and CIPN assessment methodology. ¤ - percentage extracted from one clinical study.

Notably, even though MTAs share binding domains, affinity to tubulin differs. This difference may alter the unbound intracellular concentration required to achieve pharmacologically relevant TO and exert the action of MTA (27). In the case of taxanes, docetaxel exhibited 2-fold higher affinity to tubulin compared to paclitaxel (41) and similar affinity to cabazitaxel (42). Among microtubule destabilizers, the determined affinity to tubulin followed the order: vincristine > vinblastine > vinorelbine > vinflunine (43), with eribulin showing the

least affinity to its target (44). Whether tubulin-binding affinity is one of the contributing properties of MTAs in the differences in CIPN prevalence remains unknown. The lack of data on unbound intracellular drug exposure and target engagement in CIPN-relevant tissues limits the translation of *in vitro* affinity estimates to *in vivo* neurotoxicity.

Role of biological barriers in CIPN development

CIPN sites

From the preclinical data, the PNS tissues, including dorsal root ganglia (DRG) and peripheral nerves (PN), were denoted as key CIPN sites (5, 45, 46). The pathophysiological changes in these tissues were observed after administration of 18 mg/kg of paclitaxel with two repeated doses during the week (45). Furthermore, from a functional perspective, electrophysiological measurements showed a significant decrease in nerve conduction velocity and amplitude in mice receiving multiple doses of paclitaxel and ixabepilone, but not in eribulin-treated rodents, suggesting MTAs affecting nerve functionality (47).

CIPN is primarily a PNS-related toxicity. However, CNS-related symptoms, including chemo brain, can develop due to MTA exposure in the CNS or via indirect MTA effects. The latter were observed as alterations in CNS activity, such as brain hyperactivity and neuroinflammation due to compensation for PN damage (48, 49). Therefore, the brain and spinal cord have been noted as CIPN sites (46).

Recent studies suggest that a progressive skeletal muscle (SM) disorder related to losing muscle strength (sarcopenia) is a clinically relevant risk factor for CIPN, linking impaired SM function with an increased risk of CIPN development (50, 51). Furthermore, previous studies showed extensive paclitaxel and vincristine distribution to SM (46), suggesting the need to understand the driving mechanisms of MTA distribution to the muscles.

Barriers controlling distribution of MTAs to CIPN sites

Instead of cancer cells, MTAs can distribute from blood to the CIPN sites, where it exhibits neurotoxic effects. However, the distribution to these tissues is a complex process, as drugs need to pass both endothelial and parenchymal barriers to reach their intracellular target - microtubules. In the case of CIPN sites, this includes transport across the PNS and CNS endothelial barriers, such as the blood-nerve barrier (BNB), blood-dorsal root ganglion barrier (BDB), blood-brain barrier (BBB), blood-spinal cord barrier (BSCB), and blood-skeletal muscle interface (BSMI). These barriers differ in their structure as shown in Fig. 2.

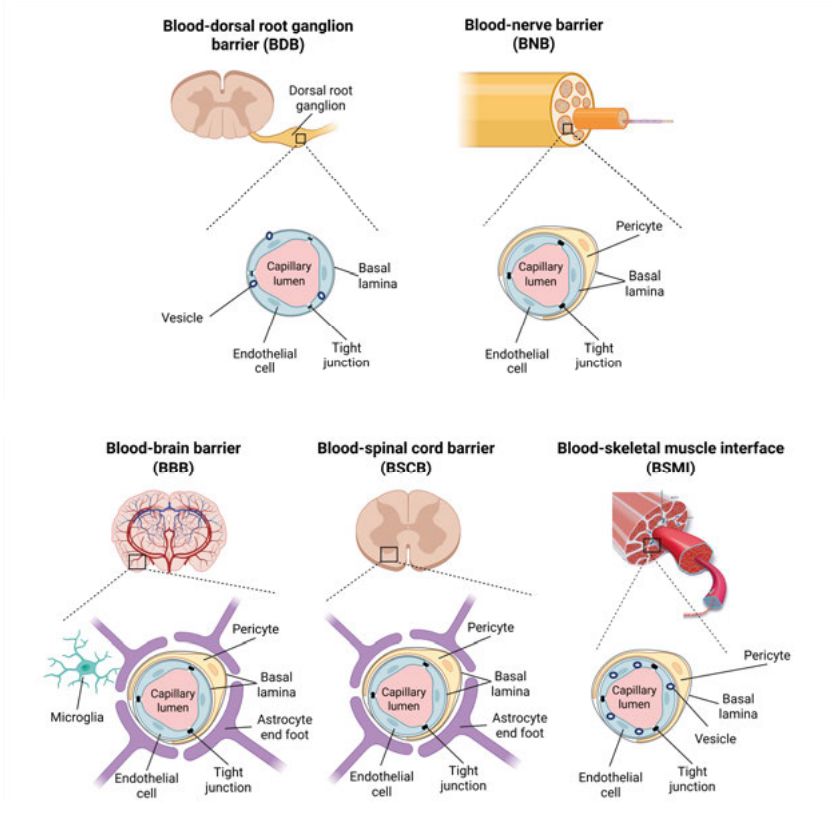

Figure 2. Anatomical differences in the endothelial barriers in the PNS, CNS, and skeletal muscle. In BDB, capillaries surrounding neuron cell bodies are fenestrated and relatively permeable with active vesicular transport, while the BNB is composed of endoneurial endothelial cells and perineurium (52, 53). BBB and BSCB are more restrictive compared to the PNS barriers, with specialized endothelial tight junctions and low transcytosis. In skeletal muscle, continuous capillaries support bidirectional exchange between plasma and the interstitial space (54). The image is modified from Hu *et al.* (46).

Recently, more extensive research has been conducted to define the structure of PNS barriers, which are less studied compared to CNS barriers (55, 56). It was shown that the BNB has a distinctive multicellular structure, conserved among species (56). In the PN, axons are enclosed by the endoneurium, with groups of them forming fascicles enclosed in the perineurium, and multiple fascicles are surrounded by the epineurium. The endoneurial blood vessels express barrier-associated transporters and tight junctions, and together with the perineurium and basal lamina form the BNB (56, 57). In the DRG, additional complexity arises due to heterogeneous structure, including a cell-body-rich area and a nerve fiber-rich area, which differ in their vascularization and BDB tightness (52, 53). Similar to BNB, BSMI is composed of several layers, including endothelium and sarcolemma, with the latter selectively regulating intracellular drug exposure (54).

MTA transport to CIPN sites

The transport of drug molecules across barriers is characterized by the rate and the extent. The rate of transport denotes how fast a drug crosses a barrier to the tissue and is estimated as influx clearance or permeability surface area product. The extent describes the drug concentration in the tissue at steady-state relative to blood (58). This thesis focuses on the extent of drug distribution.

Drug transport can occur through paracellular and transcellular pathways. Paracellular transport is restricted, accounting for 5% at BNB, BDB, 3% at BSMI, and less than 1% at BBB and BSCB, as shown using 4 kDa TRITC-dextran in healthy rats (46). The transcellular transport can be passive, carrier-mediated (facilitated or active), and vesicular (transcytosis). From this aspect, drug transporters may be an important factor in CIPN development, due to their influence on the exposure of MTAs in CIPN sites. For example, P-glycoprotein (P-gp) is an efflux transporter, highly expressed in the BBB and BSCB, therefore decreasing several MTAs' uptake into the CNS (59, 60). In a clinical study, it was shown that P-gp inhibition was associated with increased risk of CIPN, suggesting this transporter’s role in controlling the intracellular accumulation of paclitaxel in CIPN sites (61).

Some of the MTAs, like paclitaxel and docetaxel, can be substrates of several uptake transporters, including solute carrier organic anion-transporting polypeptide B1 and B3 (OATP1B1, OATP1B3) (62, 63) and organic anion transporter 2 (OAT2) (64). Their importance in CIPN development still needs to be clarified, however, there is some evidence that deficiency of Oatp1b2 in a mouse model decreases paclitaxel uptake into the DRG, and there is a lack of development of CIPN-related symptoms in mice (62). However, RNA

sequencing and proteomic studies suggest that OATP1B1, OATP1B3, and OAT2 are not expressed in human DRG (65). Thus, there is still a remaining question: which transporters are present in the PNS barriers leading to MTA accumulation in CIPN sites. Furthermore, transport across cellular barriers inside the tissue is not yet defined, but is important to consider due to the MTAs' target being intracellular.

Drug formulation effects on MTA transport

Another important aspect that can influence MTAs' distribution to the nervous system is the formulation in which MTA is used. Various formulation strategies have been developed to overcome poor solubility and formulation-related toxicity, focusing on injectable forms due to the low oral bioavailability of MTAs (66). Surfactants like Cremophor EL (CrEL) (67) and polysorbate 80 have been used to prepare infusion solutions for paclitaxel and docetaxel, respectively. In preclinical studies, it was shown that systemic pharmacokinetics of docetaxel vary between formulations consisting of different concentrations of Tween ® 80, CrEL, and dimethyl sulfoxide (DMSO) in rats (68). There are multiple paclitaxel formulations, which have been shown to have distinct plasma and tissue distribution profiles in mice (69). Authors also suggested that observed distribution profiles could explain specific formulation efficacy in particular tumor types (69). However, the formulation effect on drug distribution to the nervous system is sparse, even though it is known to influence the prevalence of CIPN in clinical settings (70).

In relation to the formulations, specifically for the taxanes, premedication is used to minimize hypersensitivity reactions, which are associated with surfactants (67). Previously, it was shown that cimetidine, one of the premedication agents, does not affect the systemic pharmacokinetics of paclitaxel (71). However, there is a lack of information if the main premedication agent, dexamethasone, has any effect on paclitaxel systemic pharmacokinetics and distribution profile. Therefore, this question needs to be further explored to understand how premedication may affect pharmacokinetic properties, including MTA distribution to CIPN sites and how it relates to CIPN development.

Methods to investigate CIPN site pharmacokinetics

The extent of drug distribution to tissues can be described using several key parameters, $K_{p,uu,tissue}$ (unbound drug tissue-to-plasma concentration ratio), and $K_{p,tissue}$ (total drug tissue-to-plasma concentration ratio) (58). The $K_{p,tissue}$ is the most often investigated parameter during drug distribution studies, including

MTAs (47, 69, 72). However, the unbound drug partition coefficient across the barriers of the CIPN sites, $K_{p,uu,tissue}$, has been investigated only for paclitaxel and vincristine (46). According to the free drug theory, only the unbound form of the drug is pharmacologically active and able to engage with the target (73). Thus, characterizing the extent of unbound MTA distribution to the nervous system is important for improving our understanding of the PK determinants of CIPN development.

Because the target of MTAs is intracellular, the unbound intracellular-to-extracellular concentration ratio, $K_{p,uu,cell}$, is another important PK parameter to evaluate (74). Altogether, $K_{p,uu,tissue}$ and $K_{p,uu,cell}$ are essential to determine MTAs' concentration in CIPN sites. These parameters can be used to estimate unbound intracellular tissue exposure relative to plasma. At steady-state, a ratio above or below unity indicates active uptake or efflux across the barrier, respectively (58). This can help refine the relationship between MTAs intracellular exposure and CIPN development, and identify transporters that contribute to MTA distribution across barriers at CIPN sites.

Approaches to investigate tissue-to-plasma ratios

The tissue partition coefficient can be estimated using two approaches: Area Under the concentration-time Curve (AUC)-based or from tissue and plasma concentrations derived at a single time point at steady-state (75). The AUC-based approach requires serial sampling to adequately characterize the concentration-time profile. Furthermore, the remaining AUC extrapolation should be no more than 20% of the full AUC in plasma and tissue. Thus, more animals need to be sacrificed for each time point compared to calculations using single concentrations at steady-state. Additionally, variability of PK parameters between individual animals over the time course is lost. Therefore, a single time point approach is more acceptable from a 3R point of view. The difficulty related to this approach is the need to reach steady-state in plasma and tissues to accurately determine concentration ratios. This may be challenging due to non-parallel concentration-time profiles in plasma and tissues, as was shown in the case of MTAs, with fast steady-state approach in plasma, but not in tissues (46).

The time needed to reach steady-state

The achievement of steady-state in plasma can be ensured by modifying the dosing regimen and monitoring it via plasma sampling. However, in the case of tissues, continuous concentration observations are often impossible due to the need for terminal sampling. The time needed to reach steady-state in

tissues is governed by multiple processes - intra-tissue distribution and elimination from tissue. Those processes are assessed by unbound volume of distribution in the tissue ($V_{u,tissue}$) and clearance out of the tissue ($CL_{out,tissue}$), respectively (76). These parameters are influenced by specific (to the pharmacological target) and non-specific binding of a drug, pH partitioning, as well as the combination of active and passive transport out of the tissue (76), which is drug- and tissue-specific. Thus, one needs to be aware of possible variability in time to steady-state concentrations in tissues between drugs and tissues themselves, and design experiments accordingly.

Assessment of intra-tissue drug distribution

Intra-tissue drug distribution encompasses drug partitioning into cells and subcellular components and binding to tissue components after passing through the barriers. This information is needed to correct available data on $K_{p,tissue}$ for tissue binding to estimate $K_{p,uu,tissue}$. The unbound drug concentration is related to the total concentration in the tissue via $V_{u,tissue}$ (mL/g tissue) (46, 77). It reflects the active uptake and drug binding into parenchymal tissue cells, but not the blood-tissue barrier transport. In the case of the brain, $V_{u,brain}$ of 0.2 mL/ g brain suggests that drug distribution is limited to interstitial fluid (ISF), and more than 1 mL/g brain shows that there is extensive tissue binding or active uptake into cells and organelles (78). $V_{u,tissue}$ is inversely correlated to the unbound fraction of drug in the tissue, $f_{u,tissue,}$ and is a more *in vivo*-like parameter, describing intra-tissue drug distribution as previously described by Fridén *et al*. with the brain as an example (79). $f_{u,tissue}$ denotes intra-tissue distribution governed by tissue binding (46, 80).

The Combinatory Mapping Approach for CIPN (CMA-CIPN)

The CMA-CIPN method (46) is based on the previously developed CMA for the brain and is based on plasma and tissue concentration determination at a single time point. CMA enabled characterization of the extent of unbound drug distribution to the brain across endothelial and cellular barriers, and determination of intracellular distribution of selected drugs (81). This approach has been used to evaluate novel drug distribution to the brain in early drug discovery phases (81), and it was upgraded to CMA-CIPN to explore distribution to CIPN sites of drugs associated with CIPN development and without reported cases of CIPN (46).

According to CMA-CIPN, $K_{p,tissue}$, determined at steady-state during *in vivo* experiments, is corrected for nonspecific tissue and plasma protein binding (75). This is done by using two separately *in vitro* determined parameters: $V_{u,tissue}$ and $f_{u,plasma}$, obtained from brain slice (77, 82) or tissue uptake (46) assays and equilibrium dialysis (80), respectively. Furthermore, combining

intra-tissue distribution data, $V_{u,tissue}$ multiplied by $f_{u,tissue}$, can be used to determine drug distribution into the cells inside the tissue (74).

Notably, CMA-CIPN is used to determine the extent of unbound drug distribution to CIPN sites as a whole tissue, but the spatial resolution is limited, especially for PN and DRG. Thus, the MTA distribution into different subregions of these tissues requires other methods to be developed.

Matrix-assisted laser desorption/ionization mass spectrometry imaging

MALDI-MSI is a label-free method that can spatially map total small- and large-molecule drug concentrations within tissue regions at a single time point (83). This is especially useful when there is a need to characterize drug distribution across anatomically or histologically distinct tissue compartments (83). MALDI-MSI has been used to visualize regional brain distribution of multiple CNS drugs, while enabling estimation of total brain-to-plasma ratio (84). The evaluation of paclitaxel distribution to tumor tissues from mice after administration of different paclitaxel formulations over time has been done via MALDI-MSI, which was consistent with the data acquired by conventional quantitative analysis (85). However, current workflows still require further methodological development, especially in spatial resolution, before they can be reliably used to detect MTA distribution in PN and DRG. Typically, MALDI-MSI can achieve spatial resolution from 20-50 µm down to 5 µm in specific cases (86), which is enough to image a whole nerve or DRG, but not the cellular or subcellular drug localization (87, 88). Furthermore, additional experiments on drug-tissue binding are needed to determine unbound concentrations of the drug inside the tissue, as this method provides total drug concentrations.

Microdialysis

The determination of unbound concentration in plasma and tissues can be done using microdialysis as a reference standard for measuring unbound drug concentrations in extracellular tissue fluid at the selected time points (89). However, this method may not be feasible to use with lipophilic molecules, like MTAs, due to nonspecific adsorption to the plastic tubing and probe (90). Solubilizers used in MTA formulations, like polysorbate 80, can form additional binding sites and disturb the quantification of concentrations in the tissues. This may hinder the determination of true MTA levels and affect the feasibility of microdialysis (91). Additionally, this method has been used to determine eribulin PK inside the brain of cancer patients (92). However, it is not possible to insert microdialysis probes into small tissues, like nerves and DRG.

Blood-based monitoring biomarkers for CIPN

In clinical settings, there is no tool to determine the early development of CIPN, therefore, most of the treatment of CIPN starts after the manifestation of CIPN-related symptoms (5). Identification of reliable blood-based biomarkers for the early prediction and monitoring of CIPN is an active area of research, as it could support timely interventions to stop CIPN progression. Several biomarkers have been explored, including brain-derived neurotrophic factor, nerve growth factor, osteopontin, peripherin, and NfL (93, 94). NfL is a potential monitoring biomarker for axonal damage, due to axonal deterioration observed during CIPN development.

NfL is a 68-70 kDa molecule that is part of the neuron cytoskeleton together with microtubules, microfilaments, and other intermediate filaments, responsible for structural integrity and axonal transport (Fig. 3) (95). It was previously shown to be a predictive biomarker in mouse models of neurodegenerative diseases, including amyotrophic lateral sclerosis and Alzheimer's disease, as reviewed by Loeffler *et al.* (96). Later, it was identified as a potential biomarker for both central and peripheral nervous toxicity in rats after administration of CNS and PNS toxicants (97).

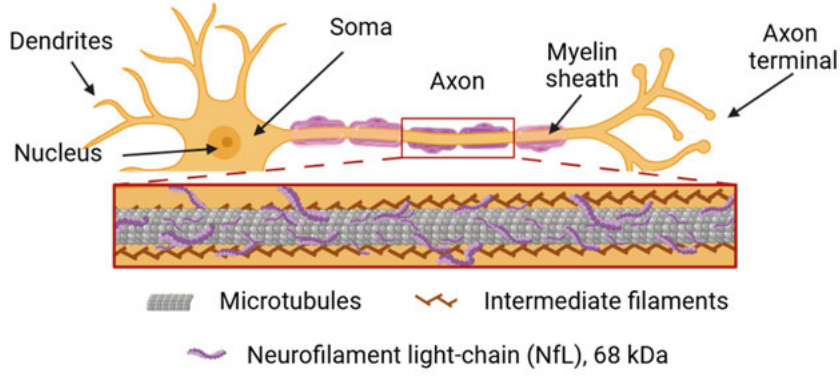

Figure 3. Overview of the neuron and cytoskeleton structure. Image constructed based on (95).

The utility of NfL as a biomarker for CIPN has been investigated in several studies. In an induced pluripotent stem cell–derived sensory neuron model, paclitaxel and vincristine showed a dose-dependent NfL increase in the medium (98, 99). In animal studies, it was shown that both repeated doses of paclitaxel and vincristine significantly increased serum NfL (sNfL) levels, with over 20- and 5-fold increases in sNfL concentration compared to the baseline in paclitaxel and vincristine treatment groups in rats, respectively (100, 101). Balayssac *et al*. also showed that the increase in NfL concentration

in plasma is directly correlated with the total cumulative dose of paclitaxel (102). Furthermore, the greatest increase in NfL was associated with increased tissue damage severity in rats (102). From a clinical point of view, Karteri *et al*. showed that a higher increase in sNfL concentrations is associated with a higher grade of CIPN after 12 months of weekly paclitaxel treatment (103). Additionally, after the first cycle of paclitaxel, patients with sNfL concentrations above 150 pg/mL were associated with the risk of paclitaxel treatment discontinuation or dose reduction due to CIPN development during paclitaxel treatment given Q3W (98).

Preclinical and clinical evidence indicates that NfL can increase during CIPN development, but the response is not uniform across administered drugs or individuals (102, 104). Therefore, to implement NfL as a monitoring biomarker for CIPN, there is a need for further research on the temporal relationship between drug exposure, biomarker release, and clinical neuropathy onset in a drug-specific manner (105).

Mathematical PKPD-biomarker modelling: focus on paclitaxel

Mathematical modeling is a useful tool for describing drug PK and its correlation with subject-related variables, i.e., demographic, laboratory values, and treatment outcomes (106). Paclitaxel is a widely used chemotherapy drug, with documented nonlinear plasma pharmacokinetics and a high prevalence of CIPN. Thus, several paclitaxel PK models have been described, including CrEL effects on paclitaxel's kinetics (107, 108), and differences in estimated PK parameters when comparing with albumin-bound (nab) paclitaxel formulation in humans (109). Mathematical models with different approaches have been made to connect paclitaxel systemic exposure to CIPN development. A population PK (popPK) model of paclitaxel and a proportional odds model on CIPN were used to identify optimal plasma sampling time to predict the time above total paclitaxel concentrations in plasma of 0.05 μmol/L do not exceeding 15 hours (110), which has been noted as a risk factor for CIPN (12). Other modeling attempts included paclitaxel popPK- and dose-response models to predict CIPN score (111, 112). However, no accurate predictor of CIPN has been demonstrated. Another study showed that PK-guided paclitaxel dosing decreased the incidence rate of neuropathy in the Asian population compared to body surface area (BSA)-guided treatment (113), further emphasizing the importance of understanding MTAs PK to lower CIPN risk in cancer patients.

To further explore and predict neurotoxic effects, simple PK models can be expanded to characterize biological processes, such as drug distribution to

the effect sites, binding to the target, and its link to observed effects (114). This has not yet been done to link paclitaxel plasma and CIPN site exposure to the observed CIPN development in patients. Thus, it is unknown if such models could better predict CIPN. Currently, no supporting human data are available to enable the development of such models. Therefore, additional preclinical studies are needed to obtain the required PK parameters to inform this relationship, which could be later extrapolated and used in paclitaxel PKPD model building using available data in humans.

Furthermore, paclitaxel PK models can be further extended to include PD parameters and biomarker information to link drug PKPD to the observed CIPN development in clinical settings. Before implementing NfL as a biomarker into mathematical models and exploring its utility, NfL kinetics and its changes due to treatment or disease progression need to be determined. An NfL model, including central and peripheral nervous system compartments, has been developed to describe NfL kinetics in healthy patients (115). This model was adjusted to describe another intermediate neurofilament, neurofilament heavy chain (NfH) kinetics in spinal muscular atrophy and treatment effect (116). A similar approach can be used to link NfL kinetics after paclitaxel administration to the paclitaxel PKPD model. Altogether, this can provide new evidence of how plasma exposure is associated with CIPN development.

Aims of the thesis

The overall aim of this thesis was to investigate the distribution and intra- and extracellular exposure of MTAs at CIPN-relevant sites using preclinical models and to integrate these findings with PKPD modelling and biomarker evaluation to improve understanding and monitoring of CIPN in cancer patients.

The specific aims were to:

- Investigate the impact of paclitaxel formulation and dexamethasone premedication on the distribution of unbound paclitaxel to CIPN-relevant sites in rats of both sexes, and to explore pharmacokinetic properties that may contribute to differences in CIPN prevalence between clinically used paclitaxel formulations (Paper I)
- Establish the relationship between paclitaxel intracellular exposure at CIPN-relevant sites and NfL kinetics using a novel semi-mechanistic PKPD model informed by experimental data and literature-derived parameters, and explore the utility of the model to simulate non-observed scenarios (Paper II)
- Using a translational PKPD modelling approach developed in Paper II, evaluate sNfL as a biomarker of PIPN by relating predicted paclitaxel exposure in plasma and CIPN-relevant sites to reported sNfL concentrations and PIPN severity assessed by the TNSc in breast cancer patients (Paper III)
- Characterize the extent of unbound eribulin distribution to CIPN-relevant sites, investigate whether its distribution may contribute to differences in CIPN incidence compared with CrEL-paclitaxel, and assess how experimental design influences the estimates of distribution (Paper IV)
- Determine the extent of unbound cabazitaxel, docetaxel, and vinorelbine distribution across endothelial ($K_{p,uu,tissue}$) and cellular ($K_{p,uu,cell}$) barriers at CIPN-relevant sites, and investigate whether differences in distribution may contribute to the varying neurotoxic potential of these MTAs (Paper V)

Material and methods

Drug selection

MTAs have been selected to explore PK determinants of CIPN development due to their known detrimental effects on the nervous system, leading to the development of CIPN in cancer patients (117). In Papers I-III, paclitaxel was chosen as the main representative drug of MTAs with a well-established high risk of CIPN (118), ongoing efforts to mitigate formulation-related side effects through the development of novel formulations (66), and an active search for diagnostic biomarkers for PIPN (119). In Paper I, dexamethasone was chosen as a typical premedication agent used during the treatment of CrEL-paclitaxel (120). In Papers IV and V, microtubule stabilizers cabazitaxel and docetaxel, and destabilizers vincristine, vinorelbine, and eribulin were selected due to their reported differences in CIPN prevalence among cancer patients (Table 1), known differences in tubulin binding properties and mechanism of action (26), as well as practical availability to acquire drugs for testing.

Animals

Male and female Sprague-Dawley rats (Taconic, Lille Skensved, Denmark) were used for the *in vivo* and *in vitro* experiments in Papers I-II and IV-V. All animals were 8-12 weeks old and weighed 250-300 g during the experiments. After arrival, rats were housed and acclimatized for one week in groups by sex under temperature- and humidity-controlled conditions, 20°C–22°C and 40%–50%, respectively, with a 12-hour light/dark cycle and *ad libitum* food and water. Experiments conducted in Paper I were performed following guidelines from the Swedish National Board for Laboratory Animals, approved by the Animal Ethics Committee of Uppsala, Sweden (Ethical Approval Dnr 5.8.18-12230/2019), and for studies described in Papers II and IV-V, the ethical approval was renewed (Dnr 5.8.18–09258/2024).

All studies were planned and conducted to minimize the use of animals and to mitigate their suffering, while ensuring enough statistical power. The sample size per group was estimated using available data on drug distribution

properties between drugs. The performed studies were not randomized or blinded for the treatment arms.

Evaluation of the unbound partition coefficient to CIPN sites

In Papers I, IV, and V, the CMA-CIPN approach was used to assess $K_{p,uu,tissue}$) and $K_{p,uu,cell}$, calculated using Eqs. 1 and 2. Thus, in these papers, *in vivo* pharmacokinetic studies and *in vitro* equilibrium dialysis, brain slice and tissue uptake experiments were performed.

$$K_{p,uu,tissue} \approx \frac{K_{p,tissue}}{V_{u,tissue} \, x \, f_{u,plasma}} \quad (1)$$

$$K_{p,uu,cell} = V_{u,tissue} \, x \, f_{u,tissue} \quad (2)$$

Where $K_{p,tissue}$ is the total tissue-to-plasma ratio in the tissue of interest, $V_{u,tissue}$ is the unbound volume of drug distribution in the tissue, $f_{u,plasma}$ is the fraction of unbound drug in plasma, and $f_{u,tissue}$ is the fraction of unbound drug in a tissue.

In Paper V, to further assess the connection between different MTAs' exposure in plasma and tissues and their tubulin binding properties, relative TO was estimated in sciatic nerve (SN), chosen as a representative tissue of PN, DRG, SM, and brain (Br). This was done by utilizing unbound partition coefficients across endothelial and cellular barriers for each MTA determined during this thesis and the equilibrium dissociation constant (K_d), reported in the literature for each MTA, using Eq. 3:

$$TO = \frac{C_{tot,plasma}{}^{\gamma}}{(K_d / f_{u,plasma} \, x \, (K_{p,uu,tissue} \, x \, K_{p,uu,cell}))^{\gamma} + C_{tot,plasma}{}^{\gamma}} \quad (3)$$

Where γ is the Hill coefficient, and is assumed to be 1.0. The acquired estimates of TO were used to compare MTAs' occupancy levels at different total and unbound concentrations in plasma and target sites.

Total tissue distribution

In order to determine the $K_{p,tissue}$ for different MTAs, 4-hour constant-rate IV infusions were performed in male and female rats. The samples collected at the single time point at the end of infusion were used to calculate $K_{p,tissue}$.

Dosing regimen selection

To ensure steady-state plasma concentrations at the time of sampling, MTAs were administered intravenously as a combination of a loading and a maintenance dose. They were calculated using the total targeted plasma concentration at steady-state ($C_{tot,plasma,ss}$), steady-state volume of distribution (V_{ss}), and the clearance (CL) of the specific MTA, respectively. The choice of the total dose and $C_{tot,plasma,ss}$ was based on available data on $C_{through}$ observed in clinical settings during common dosing regimens of specific MTAs, maximum tolerated doses, acceptable infusion rate and volume in rats, and manufacturers' instructions on preparing the infusion solution.

Experimental procedure

The day prior to the experiment, the surgery was performed under anesthesia by inhalation of isoflurane with oxygen. During the surgery, catheters in the femoral artery and vein were placed to enable hourly sampling of plasma and constant-rate infusion, respectively. After catheterization, rats were individually placed into a CMA120 system for freely moving animals with *ad libitum* access to food and water.

During the experiment, an infusion solution of a specific MTA was administered at a predetermined rate for 4 hours, and plasma samples were collected every hour to assess the achievement of steady-state plasma concentration of MTAs. At the end of each experiment, the rats were put under anesthesia of isoflurane and oxygen. In Paper IV, cerebrospinal fluid (CSF) was collected from the *cisterna magna*. In Papers I-II, IV, and V, terminal blood was collected via cardiac puncture, and tissue sampling was done after decapitation. The tissue samples included SN, DRG, SM, Br, and spinal cord (SC). All tissue samples were weighed and homogenized with phosphate-buffered saline (PBS) with either nine (SN, DRG), four (SM), or three (Br, SC) volumes of buffer per tissue weight. The homogenates were stored at −80 °C pending bioanalysis to later quantify total tissue concentration of administered MTA.

Intra-tissue distribution

In Papers IV and V, the unbound volume of distribution of MTAs in the brain ($V_{u,br}$) and other CIPN sites ($V_{u,SN}$, $V_{u,DRG}$, and $V_{u,SM}$) were evaluated using brain slice and tissue uptake assays, respectively (46, 77, 121). These methods have been previously developed to connect total drug concentration in the tissue and unbound drug concentration in artificial extracellular fluid (aECF), which mirrors the tissue interstitial fluid concentration of the drug *in* vivo, under *in vitro* conditions. After sacrificing drug-naïve rats, SN, DRG, SM, and Br were immersed in ice-cold oxygenated aECF. During the brain slice assay,

six 300 µm coronal slices were obtained from each rat brain using a vibrating-blade microtome Leica VT1200, and then transferred into a Ø80-mm flat-bottomed glass beaker. In the case of tissue uptake assays, the amount of tissue used was scaled down to approximately 15 mg of SN, DRG, and SM, and brain as a reference, which were transferred to a 24-well polystyrene plate. Both in the beaker and plate tissues were immersed in aECF, containing 100 nM of a selected MTA.

These experiments were performed for 5 hours by incubating tissues at 37 °C in an orbital shaker MaxQ4450. At the end of incubation, buffer, brain slices, and tissues were collected. Brain slices and tissues were dried, individually weighed, and homogenized using aECF (1:9, w:v), buffer samples were mixed with blank brain homogenates in aECF to match matrixes. At 5 hours, it was assumed that equilibrium was reached and $V_{u,tissue}$ was calculated using the MTA amount in the tissue (A_{tissue}) and the unbound MTA concentration in the buffer ($C_{u,buffer}$), corrected for the residual volume of aECF, surrounding the tissue (V_i), as shown in Eq. 4:

$$V_{u,tissue} = \frac{A_{tissue} - C_{buffer} \times V_i}{C_{buffer} \times (1 - V_i)} \quad (4)$$

A V_i was obtained previously for brain, SN, and DRG by using the marker ^{14}C-sucrose (46). Thus, the values of 0.133, 0.146, and 0.122 mL/g tissue, respectively, were used for calculations. For SM, the V_i was presumed to be the same as for SN, and SC was assumed to have the same $V_{u,tissue}$ as the brain.

Plasma and tissue binding

In Papers I, IV, and V, the equilibrium dialysis method was used to investigate the fraction of unbound MTAs in plasma ($f_{u,plasma}$) and in the CIPN sites, $f_{u,Br}$, $f_{u,SC}$, $f_{u,SN}$, $f_{u,DRG}$, and $f_{u,SM}$, according to the method by Kalvass and Maurer (80), with modifications. For the determination of $f_{u,plasma}$, plasma samples from *in vivo* pharmacokinetic studies were used, enabling assessment of the impact of the paclitaxel formulation on the fraction unbound (Paper I), and the plasma binding properties of different MTAs in individual male and female rats (Papers I, IV, and V). Tissue samples were obtained from drug-naïve male rats and homogenized in PBS (1:9, w:v) before the experiment. All samples were spiked to reach the final concentration of 1000-2000 nM, depending on the tested MTA, due to previously reported high binding to plasma proteins and the need to be able to quantify the unbound MTA concentrations in the buffer side.

A Teflon 96-well plate HTD96b with a regenerated semipermeable cellulose membrane (12-14 kDa) was used for these experiments. During the dialysis, equal volumes of spiked matrixes and PBS were placed on opposite sides of the membrane and dialyzed for 6 hours at 37°C and 200 rpm in a MaxQ4450 incubator. At the end of the experiment, plasma, tissue, and buffer samples were collected, matrix-matched, and stored at -20 °C before bioanalysis. The fraction of unbound drug was calculated as the ratio of unbound drug concentration in the buffer to the total concentration in the corresponding plasma or tissue sample, using Eqs. 5 and 6, respectively.

$$f_{u,plasma} = \frac{C_{receiver}}{C_{donor}} \quad (5)$$

$$f_{u,tissue} = \frac{\frac{1}{D}}{\left(\frac{C_{donor}}{C_{receiver}} - 1\right) + \frac{1}{D}} \quad (6)$$

Where D is the dilution factor, equal to 10, and C_{donor} and $C_{receiver}$ are the determined concentrations on either the donor or receiver side.

Assessment of steady-state attainment in CIPN sites

During *in vivo* experiments, plasma concentrations of MTAs can be monitored. However, this cannot be done at the tissue level due to the need for terminal sampling to obtain tissues of interest. This can be mitigated by either increasing the number of animals used per study and sampling times or by estimating the achievement of steady-state in tissues *in silico*. Thus, in Papers IV-V, using Berkeley Madonna v10.2.8, a simplified distribution model was built to simulate constant-rate infusions of different MTAs and assess the time needed to reach steady-state concentrations in CIPN sites.

The model included one plasma compartment linked to DRG (Paper IV) and brain (Paper IV-V) compartments, chosen as relevant tissues of the greatest and lowest extent of unbound drug distribution in the PNS and CNS, respectively (46). MTAs PK were described using V_{ss} and CL obtained from the literature, and $f_{u,plasma}$, $f_{u,tissue}$, and $V_{u,tissue}$ were determined experimentally and reported in this thesis. MTA distribution across BDB and BBB was described as the net influx ($CL_{in,tissue}$) and efflux ($CL_{out,tissue}$) clearances of unbound MTA. The net influx was derived from calculated octanol/water partition coefficient (cLogP) values, while the net efflux was estimated from available data on MTA PK in the DRG and brain, as shown in Eq. 7.

$$K_{p,uu,tissue,ss} = \frac{CL_{in,tissue}}{CL_{out,tissue}} = \frac{P \; x \; SA}{k_{el,tissue} \; x \; V_{u,tissue}} \quad (7)$$

Where P is drug permeability (cm/s), SA is the surface area of endothelial cells in the tissue (cm^2/g tissue), and $k_{el,tissue}$ is the tissue elimination constant (1/h), calculated from literature data on MTA PK in tissues. Using the sets of different parameters for each investigated MTA, unbound tissue-to-plasma concentration ratios over time were simulated and compared with $K_{p,uu,tissue,4h}$ derived experimentally. The separate combinations of parameters with which the observed $K_{p,uu,tissue,4h}$ of different MTAs could be fitted were identified. Then selected net influx and efflux clearances were used to calculate $K_{p,uu,tissue,ss}$ (Eq. 7), while $k_{el,tissue}$ was utilized to determine the time needed to reach steady-state in the tissue (Eq. 8).

$$t_{1/2,tissue} = \frac{0.693}{k_{el,tissue}} \quad (8)$$

NfL kinetics after bolus paclitaxel administration

In Paper II, a 10-day longitudinal experiment was performed in male rats to generate data on NfL kinetics after a single 10 mg/kg bolus dose of CrEL-paclitaxel via the tail vein. Serum samples were collected from the hind leg before paclitaxel injection and every 24 hours post-injection in the morning. At 72- and 240-hour post-injection, terminal sampling was performed under anesthesia with isoflurane balanced with oxygen. Collected samples included CSF from the *cisterna magna*, serum from cardiac puncture, SN, DRG, and hippocampus. Furthermore, control animals were injected with saline, and pre- and post-injection serum samples were collected together with other tissue samples after injection to set the baseline of NfL concentrations in the serum, CSF, SN, DRG, and hippocampus. The tissue samples were weighed, mechanically homogenized in RIPA buffer with protease inhibitors, using either four (hippocampus and SN) or nine (DRG) volumes of buffer per tissue weight. Then, samples were centrifuged, and the supernatant was further stored at -80 °C before bioanalysis.

Bioanalysis

UPLC-MS/MS

In Papers I, IV-V, a liquid chromatography tandem mass spectrometry method was utilized to quantify different MTAs and their respective internal standards in various matrices, including plasma, CSF, and homogenates of SN, DRG, SM, Br, and SC. The sample analysis was done using Acquity ultra-performance liquid chromatography coupled with a Xevo TQ-S Micro triple quadrupole mass spectrometer (Water Corporation). For all compounds, quantification was performed using multiple reaction monitoring mode to monitor Parent → Product ion m/z transitions. Chromatographic separation was completed using a gradient elution method, while mass spectrometric analysis was done using the electrospray ionization method.

The analytical method for each MTA was developed by optimizing system parameters to identify and quantify each drug. External standards were matrix-matched to the type of sample, and a co-eluting internal standard method was used. Data acquisition and quantification were performed using MassLynx v4.2 (Water Corporation). All calibration curves were fitted to match expected MTA concentrations in the sample sets and to demonstrate good linearity ($R^2 \geq 0.99$). At least three levels of quality control samples were included and distributed across the calibration curve range.

The sample preparation for bioanalysis was performed by including samples of different matrices, respective calibration standards, quality control samples, and respective blanks. The preparation was done in two steps: protein precipitation and dilution.

Automated Immunoassay System

In Paper II, to quantify NfL concentrations in serum, CSF, hippocampus, DRG, and SN samples, a Simple Plex Rat NF-L Cartridge with Ella™ Automated ELISA was utilized. Sample dilution was performed on the day of bioanalysis, with a 1:1 (v:v) dilution of serum or CSF sample with sample diluent. A dilution optimization was performed for tissue samples using serial dilution to determine the optimal dilution factor for each tissue. The dilution factor used for hippocampus and peripheral tissues (SN, DRG) was 1000 and 800000, respectively, to fit detectable sample concentrations within the internal calibration range.

Statistical analysis

In Papers I-II and IV-V, statistical analysis was done using GraphPad Prism software (version 9.3.1 for Windows). Multiple data sets were compared by treatment or tissue. Thus, statistical tests were chosen to fit the objective of analysis. Normality tests were done to check normal data distribution before selection of the statistical methods. Overall, one- or two-way ANOVA followed by multiple comparison tests were utilized for comparing multiple groups. In Paper II, a mixed-effects analysis was done to compare NfL concentration in tissues. In Paper IV, multiple t-tests were chosen instead due to the comparison of two treatment groups. A $p < 0.05$ was set as a significant difference, and data were presented as mean values and standard deviations unless specified in another way.

Mathematical modeling

In Papers II and III, a non-linear mixed-effects modelling (NLME) approach was utilized to describe the distribution of CrEL-paclitaxel in plasma and CIPN sites. Using this approach, the paclitaxel exposure in CIPN sites was connected to NfL kinetics in rodents, and the connection between sNfL and the TNSc were investigated in cancer patients.

Data analysis and simulation were done utilizing NONMEM (122) (version 7.5.1), executed via Perl-speaks-NONMEM (PsN) (123) version 5.2.6. In Paper II, parameters were estimated using the first-order conditional estimation method with interaction (FOCEI), whereas in Paper III, the stochastic approximation expectation maximization (SAEM) algorithm with the Laplace method was used.

Data used for modelling purposes

In addition to the generated data in Papers I-II, datasets from other preclinical and clinical studies were included. Other sources included *in vivo* data on total paclitaxel exposure in plasma, tissues and sNfL measurements in rodents after different dosing regimens of paclitaxel for Paper II. Furthermore, data from an observational study in breast cancer patients receiving paclitaxel, reporting longitudinal NfL and TNSc data, were acquired for Paper III. This dataset included sNfL and TNSc data at baseline and at 2, 3, and 12 weeks post the start of weekly 1-hour IV infusion of paclitaxel (80 mg/m^2) in chemotherapy-naïve cancer patients (n=49). The summary of included data sets is presented in Table 2.

Table 2. Summary of dependent variables in data sources used in Paper II-III. Abbreviations: SN – sciatic nerve, DRG – dorsal root ganglion, Br – brain, NfL – neurofilament light chain, CSF – cerebrospinal fluid, TNSc – Total Neuropathy Score-clinical version.

Paper	Dependent variables	Species	Data sources
Paper II	Total paclitaxel concentration in plasma, SN, DRG, Br NfL concentrations in serum or plasma, CSF, SN, DRG, Br	Rodents (mice, rats)	(46, 47, 124-127)
Paper III	NfL concentrations in serum TNSc data	Humans	(103)

Model building workflow

In Paper II, one-, two-, and three-compartment PK models were tested in describing total paclitaxel plasma concentration and saturable distribution to the tissues. Due to known nonlinear paclitaxel kinetics in the central compartment, CrEL PK was included utilizing its human model from the literature, allometrically scaled by body weight (108, 128). Each tissue compartment, i.e., SN, DRG, and Br, was described with extra- and intracellular components. The extent of paclitaxel distribution into the tissue was governed by previously reported tissue-specific $K_{p,uu,tissue}$, in the model, defined as the ratio of the net influx and efflux clearances. The transport across cellular barriers was described using $K_{p,uu,cell}$. Both values were fixed to previously experimentally derived values (46). Intracellular paclitaxel-tubulin binding was noted using capacity-limited kinetics (129). This complex was linked to the NfL release from the tissues into the CSF and serum following paclitaxel administration, and linear and non-linear relationships were tested to describe the drug effect. The general NfL kinetics were characterized using turnover models.

In Paper III, a paclitaxel PK model, developed using data from rodents in Paper II, was allometrically scaled to humans. $K_{p,uu,tissue}$ and $K_{p,uu,cell}$ were assumed to be the same between species, while weights of PN, DRG, and Br were adjusted to human-relevant values based on literature data. Total and unbound plasma concentrations of paclitaxel in cancer patients were predicted using previously published popPK models (108, 128), whereas NfL kinetics were described in a similar way as in Paper II, with NfL release being driven by total intracellular paclitaxel-tubulin complex within all tissues included in the model. The mixture functionality ($MIX) was used to describe NfL kinetics differences identified among patients. A bounded integer (BI) model was used to characterize the longitudinal TNSc and its connection to sNfL, with

the assessment of effect delays. Covariate analysis was performed to test age, body mass index, and body surface area.

The performance of the model was evaluated using the physiological plausibility of the parameter estimates, the size of relative standard errors (RSE), derived from Sampling Importance Resampling (SIR), the objective function value (OFV, i.e., − 2·log-likelihood) to compare between two models, and graphical evaluation. The latter included visual predictive checks (VPC), where experimental data were compared with the data generated from simulated replicates based on the model and study design.

In Papers II and III, the developed model was used to simulate paclitaxel concentration in plasma and tissue compartments after different dosing regimens. Furthermore, models were used to explore each tissue's contribution to the observed elevation of sNfL concentrations.

In Paper III, the final model was used to evaluate the impact of age on the severity of PIPN via simulations of patient groups within different age groups. An individual dynamic prediction (IDP) was performed to identify the model's ability to predict sNfL and TNSc changes over time. The AUC of the receiver operating characteristic (ROC) metric was utilized to assess how the model separates patients at low and high risk of severe CIPN using sNfL data.

Results and Discussion

From paclitaxel distribution to NfL-guided CIPN prediction

Formulation and premedication impact on MTA distribution

To understand the drug formulation effect on the extent of unbound paclitaxel distribution across endothelial barriers to CIPN sites, three paclitaxel formulations were tested using CMA-CIPN in rats. These included CrEL-paclitaxel, nab-paclitaxel, and paclitaxel in XR17 micelles (micellar-paclitaxel). Furthermore, two dose levels of dexamethasone were used to explore its effect on CrEL-paclitaxel distribution to CIPN sites.

In Paper I, a lower extent of unbound paclitaxel distribution was revealed in the CrEL-paclitaxel treatment arm compared to other formulations across all CIPN sites. In rats at the 4-hour sampling time point, the most prominent difference was observed at BNB, BDB, and BSCB. At the PNS sites, the $K_{p,uu,tissue}$ were 0.89, 1.41, and 1.71 across BNB and 0.27, 0.71, and 0.60 across BDB for CrEL-, nab-, and micellar-paclitaxel, respectively. This difference between formulations was driven by a more than 2-fold higher $K_{p,tissue}$ and 2-fold higher $f_{u,plasma}$ values determined in CrEL-free formulations, while the $V_{u,tissue}$ was assumed to be the same between formulations. In the case of premedication, within selected dexamethasone doses given 30 min prior to the CrEL-paclitaxel infusion via hind leg, no difference in the unbound partitioning to CIPN sites was observed, except across BDB between CrEL-paclitaxel alone and with 0.15 mg/kg dexamethasone premedication, with $K_{p,uu,DRG}$ of 0.27 and 0.60 ($p = 0.019$), respectively.

Compared to previous published studies (46), in this work male and female rats were included, showing no sex difference in the PK parameters of paclitaxel independent of its formulation. There are several active transporters of paclitaxel that have been suggested to play an important role in its uptake in the PNS and extensive efflux in CNS tissues. It is a substrate of the efflux transporter P-gp (61) and some influx transporters, like OATP1B1, OATP1B3 (62, 63), and OAT2 (64). It was suggested that their expression and activity at CIPN sites could govern observed differences in the distribution between tissues in rodents. This is not clearly established in humans. In addition, nab-

paclitaxel is suggested to be able to use the albumin receptor to activate caveolae-mediated endothelial transcytosis (130). However, its effect on the extent of distribution is unclear.

In this thesis, $K_{p,uu,tissue}$ for paclitaxel formulations to CIPN sites were determined, while in the literature only $K_{p,tissue}$ for Br and SM were reported (69). $K_{p,tissue}$ values were derived using an AUC-based approach in female mice after a 10 mg/kg single dose of different paclitaxel formulations (69). The direction of differences between formulations is in line with the data presented in Paper I. In contrast to the mice data, Paper I reported $K_{p,tissue}$ values in rats that were at least 7-fold higher compared to those in mice (69). However, it is unclear if this is due to differences in species or the total dose of paclitaxel given. Previously, similar $K_{p,tissue}$ values were reported in male rats in the wide dose range (0.18-4.5 mg/kg), confirming lack of dose-dependence in the investigated range (46).

NfL kinetics after paclitaxel administration

To understand paclitaxel effects on NfL kinetics, in Paper II a longitudinal study was employed in male rats. The final study design included the observation of NfL changes in serum, CSF, SN, DRG, and cerebellum over 10 days after a single bolus CrEL-paclitaxel dose via the tail vein. In this thesis, a method to quantify NfL concentrations in the PNS tissues was optimized in collaboration with the SciLifeLab Affinity Proteomics Platform.

During the pilot studies, a 10 min IV infusion of 10 and 15 mg/kg of paclitaxel dose levels was tested. Due to a 50% mortality rate of rats receiving the higher paclitaxel dose, the 10 mg/kg dose was selected for further experiments. Bioanalysis of serum samples from the pilot revealed that surgery, like catheterization, increases baseline sNfL concentrations almost 10-fold compared to healthy controls, 312.6 and 28.4 pg/mL, respectively (Fig. 4A). Similar results were shown in mice 24 hours after tibial fracture surgery, with sNfL elevated by ~ 5-fold compared to the baseline (131). Furthermore, isoflurane, used for anesthesia, was shown to increase BBB permeability and sNfL levels by ~ 4-fold in mice after 30 min of anesthesia with 2.5% isoflurane (132). Therefore, the longitudinal study was designed as a bolus injection of paclitaxel via a tail vein to mitigate the effect of surgery on sNfL levels. Furthermore, serum samples taken at the end of the study, before and after the 20 min anesthesia using 2.5% isoflurane, showed that the sNfL variability between samples at 240 hours was within 2-fold (mean values of sNfL before and after anesthesia being 94.3 and 57.3 pg/mL, respectively) (Fig. 4B), with the observed trend of decreasing rather than increasing, as reported previously (132).

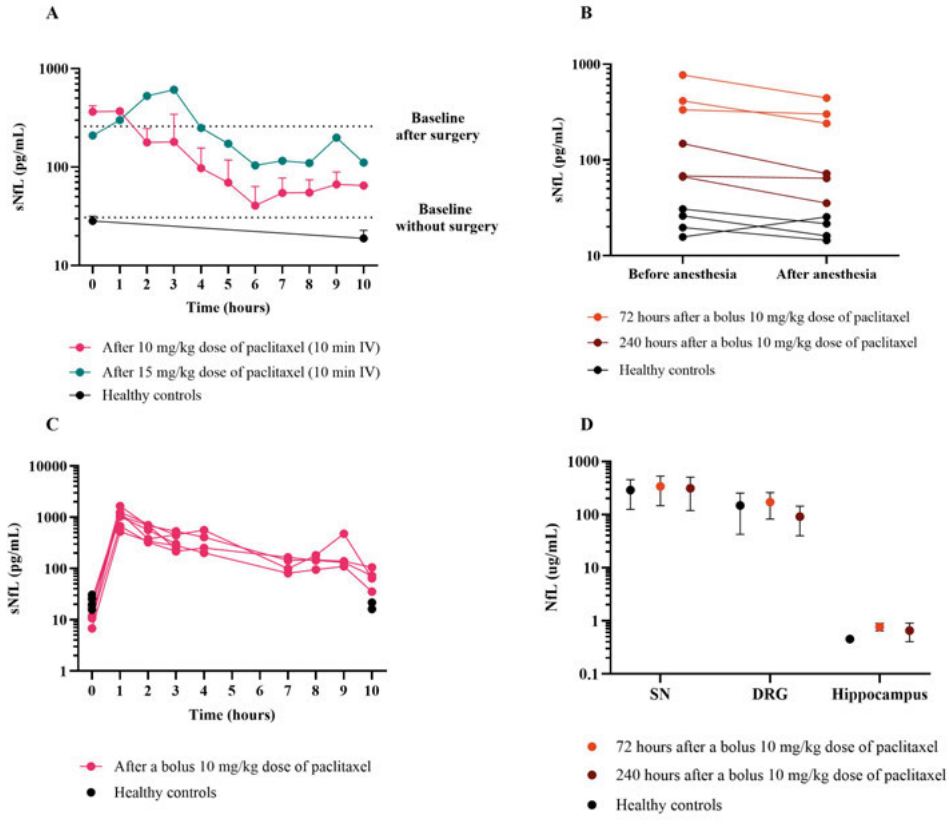

Figure 4. Semilogarithmic plots showing neurofilament light-chain (NfL) kinetics after paclitaxel administration in male Sprague-Dawley rats. (A) Serum NfL (sNFL) concentration changes over 10 days after a short 10 min IV infusion of 10 mg/kg (magenta, N=2) or 15 mg/kg (green, N=1) of paclitaxel via vein catheter compared to healthy controls (black) in the pilot study. Horizontal dotted lines show mean baseline sNfL concentration after the surgery or without the surgery. (B) Determined sNfL concentrations before and after 20 min anesthesia with 2.5% isoflurane balanced with oxygen, 72 (light brown) and 240 (dark brown) hours after a bolus 10 mg/kg dose of paclitaxel via the tail vein compared to the healthy controls, injected with saline (black). (C) sNfL concentrations over time after administration of a single dose of 10 mg/kg paclitaxel (magenta), or saline (black) via the tail vein. (D) NfL concentrations in sciatic nerve (SN), dorsal root ganglia (DRG), and hippocampus before (black) and 72 (light brown) and 240 (dark brown) hours after a bolus 10 mg/kg dose of paclitaxel via the tail vein. Note the difference in NfL concentrations between serum and tissues.

An NfL increase in serum and CSF was observed in the first days after a bolus paclitaxel dose via the tail vein. Twenty-four hours post-paclitaxel injection, sNfL was over 60-fold higher in serum compared to the baseline (Fig. 4C), while NfL levels in CSF remained increased by ~ 2-fold at 72 and 240 hours compared to the baseline. At the end of the experiment, sNfL remained

elevated with a 4-fold difference compared to the sNfL concentration before paclitaxel administration. This sNfL response to paclitaxel is in line with clinical data, showing higher-than-baseline levels of sNfL after paclitaxel treatment cessation, which could be explained by its long apparent elimination half-life of 43 days (98).

In this thesis, it was the first attempt to quantify absolute NfL concentrations in the PNS tissues. Thus, the available bioanalytical method was further adapted to enable NfL detection in the tissues. At least a 400-fold higher NfL pool was determined at the PNS sites compared to the hippocampus, with baseline concentrations of 355.1, 183.6, and 0.43 μg/mL in SN, DRG, and hippocampus, respectively (Fig. 4D). The reasons behind the observed inter-individual variability in NfL tissue concentrations are unknown. There were insignificant differences in NfL concentration changes after a bolus paclitaxel injection, however, a slight decrease was observed in the DRG between 72 and 240 hours, and a trend of increased concentrations in the hippocampus, compared to the baseline.

Paclitaxel PK and NfL kinetics model

To further explore the effect of paclitaxel on the observed NfL kinetics in rodents, a semi-mechanistic model was developed to describe paclitaxel plasma-CIPN sites exposure and its link to NfL release from the nervous system. The developed model was then used to simulate paclitaxel and NfL kinetics after different dosing regimens and explore separate tissue contributions to NfL kinetics.

In Paper II, a two-compartment paclitaxel PK model with linear and non-linear distribution processes, together with a paclitaxel-CrEL binding model, best described paclitaxel plasma data in rodents (Fig. 5A). Every CIPN tissue included in the analysis was described with one compartment, except the brain, which required a two-compartment model to better describe the data. The increase in systemic paclitaxel exposure due to the repeated dosing regimen significantly increased maximum cellular tubulin binding capacity to paclitaxel, which is in line with the literature data (133). This was described using a Hill function in the DRG and brain and an exponential function in the PN compartment. The most extensive clearance of paclitaxel out of the tissue was observed in the PN, with $CL_{out,tissue}$ being 772.5, 23.7, and 0.577 μL/h in the PN, brain, and DRG, respectively.

In the semi-mechanistic model, the incorporated NfL kinetics description included two NfL pools, i.e., the PNS, with combined PN and DRG, and CNS. The CSF and serum compartments were denoted using turnover models. The leakage of NfL from the brain through CSF or from the PNS straight to the

serum was described using a linear function, driven by intracellular paclitaxel-tubulin complex formation (Fig. 5B).

The developed model expanded the ability of previously published models (107, 108) by predicting paclitaxel exposure in the CIPN sites. In the literature, most models focused on describing the nonlinearity of systemic paclitaxel kinetics due to CrEL, including distribution to peripheral compartments (107, 108, 134). In the model built during this thesis, tissue-specific parameters were included, like unbound partition coefficients and estimated tissue weights, which enabled efficient estimation of experimentally observed data in plasma and CIPN sites. The model could predict paclitaxel accumulation in tissues, as reported by Wozniak *et al.*, who showed that there are detectable paclitaxel concentrations both in SN and DRG 60 days after treatment cessation (47). Due to the model structure, it could predict intracellular paclitaxel exposure, which is important for understanding the level of pharmacologically active paclitaxel concentration in CIPN sites.

The paclitaxel-tubulin complex was selected as a driving force behind NfL leakage from the nervous system to the serum due to the known microtubule-stabilizing effect of paclitaxel. *In vitro* data on DRG neurons show that higher paclitaxel concentration leads to increasingly more axon swelling over 72 hours, as a relevant mechanism associated with CIPN development (135). The integrated paclitaxel PK-NfL model could predict sNfL levels after different dosing regimens as shown in Paper II, slightly underpredicting sNfL after higher doses of paclitaxel, suggesting additional mechanisms underlying sNfL leakage.

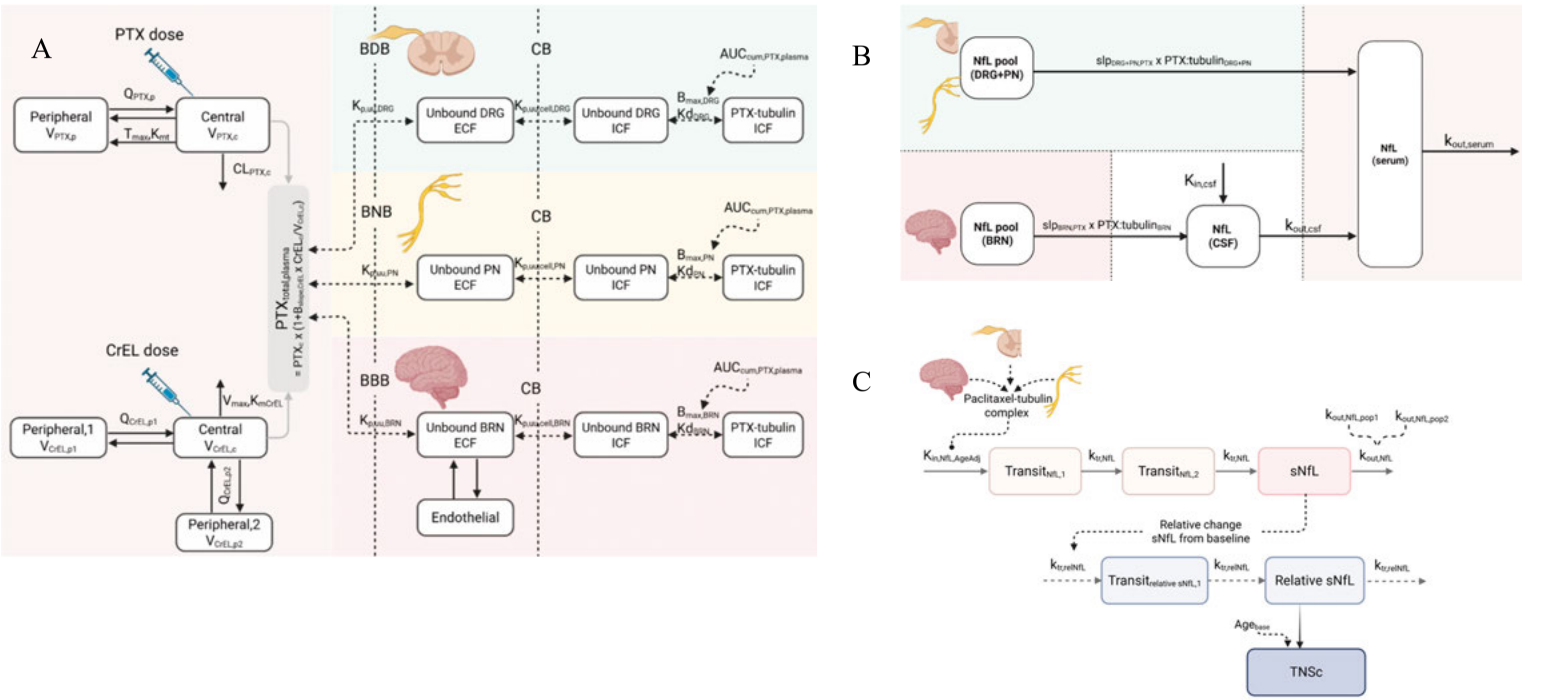

Figure 5. Schematic representation of the paclitaxel PK-NfL model. (A) Integrated plasma-CIPN sites model of paclitaxel and Cremophor EL. Solid arrows showing mass transpoer, and dashed arrows – no mass transfer. (B) Neurofilament light-chain (NfL) kinetics model in rodents. (C) Paclitaxel PK – sNfL – TNSc model in cancer patients. See the explanations of parameters in Papers II and III. Abbreviations: PK – pharmacokinetics, NfL – neurofilament light-chain, CIPN – chemotherapy-induced peripheral neuropathy, TNSc – total neuropathy score-clinical version.

CIPN prediction via paclitaxel PK-NfL-TNSc model

To translate the knowledge on paclitaxel plasma-CIPN sites exposure and NfL kinetics, a semi-mechanistic model based on rodent data was adapted to estimate paclitaxel exposure and NfL kinetics in cancer patients. Furthermore, using clinical data on sNfL and TNSc score over time, sNfL use as a predictive biomarker for CIPN development was evaluated.

In Paper III, the paclitaxel PK model from Paper II was adapted to predict paclitaxel exposure in plasma and tissue in cancer patients. The paclitaxel PK-sNfL model included a turnover model combined with two transit compartments (Fig. 5C). The total paclitaxel-tubulin complex across all CIPN sites affected NfL leakage from the tissues over time, described in an Emax function. By using a mixture model, two patient subpopulations were identified with slightly different sNfL kinetics. The baseline sNfL concentrations were correlated with age, which was shown to be the most important variable affecting sNfL concentrations among patients (136, 137). Of all patients, 31% of them (Subpopulation 2) showed a longer sNfL half-life compared to the rest of the patients (Subpopulation 1), with mean values of 112 and 42 days, respectively, after an 80 mg/m^2 Q1W dosing regimen. Using the model, a 175 mg/m^2 Q3W dosing regimen was simulated, and the apparent sNfL half-life was identified to be longer, with values of 76 and 135 days for Subpopulations 1 and 2, respectively. The estimated parameter for Subpopulation 1 was similar to the previously reported median apparent elimination half-life of approximately 43 days (interquartile range of 27–82 days) following the discontinuation of paclitaxel exposure after 175 mg/m^2 Q3W (98).

The progression of TNSc over time was described using the latent variable ($TNSc_{LV}$) within the BI model. The changes in the variable were due to baseline age and the relative change of sNfL from the baseline ($E_{Nfl,rel}$). The latter was described using an Emax function with two delay compartments. Thus, using the model, 13 days delay in sNfL increase could be captured. This can be attributed to the fact that NfL is a subacute-to-chronic biomarker in the case of traumatic brain injury, with observed gradual concentration increase over weeks post-injury (138).

After generating 1000 patients to assess age impact on the severity of PIPN, the model revealed that, compared to the patient group aged 49-64, CIPN grades 2-4 were more experienced by patients aged 65-78 (164%) and less by patients aged 34-48 years (44%). Landmark analysis showed that, depending on the age group, sNfL and TNSc data could better or worse predict CIPN severity at 12 weeks (Fig. 6). Data recorded up to 4 weeks yielded an ROC AUC of approx. 0.6 in the patient group aged 34-48, and up to 0.65 in the patient group above 65 years in both subpopulations.

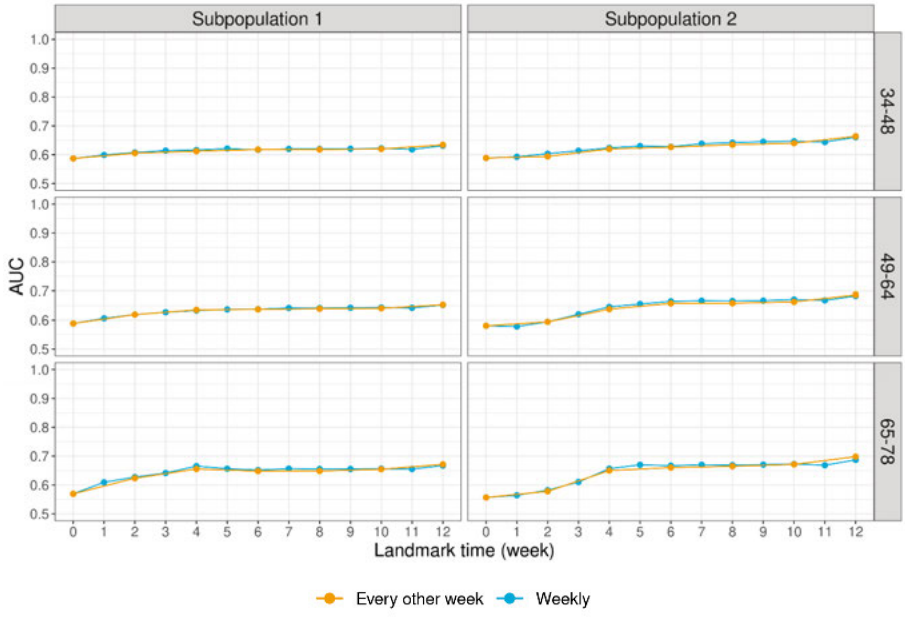

Figure 6. The area under the Receiver Operating Characteristic (ROC) curve (AUC) at 12 weeks for Subpopulations 1 and 2, stratified by follow-up frequency for landmark times for every other week follow-ups (orange) and for weekly follow-ups (blue). The panels illustrate the different age groups. Abbreviations: sNfL, serum neurofilament light chain; TNSc, the total neuropathy score clinical version.

The contributing role of tissues to the elevation of sNfL

In Papers II-III, the paclitaxel PK model consisted of the description of PN, DRG, and brain compartments, therefore, using the model, the contributing role of each CIPN site could be evaluated. In Paper II, using rodent data, PN were identified as the relatively prominent contributor to sNfL kinetics, compared to the DRG and brain. On the contrary, in Paper III, the human model predicted the brain as the main contributor. This difference may be due to differences in tissue size between species.

Distribution to CIPN sites and tubulin engagement of MTAs

Time needed to reach steady-state in tissues among MTAs

To understand the temporal aspect of MTAs' distribution to CIPN sites, and evaluate the generated data on $K_{p,uu,tissue,4h}$, a model was built to simulate the course of MTA distribution to the PNS and CNS. In Papers IV-V, due to the

availability of the data, only the time to reach steady-state concentrations in the brain could be estimated for all selected MTAs.

Simulation results showed that MTAs differ in the estimated length of constant-rate infusion needed to reach steady-state (Table 3). A 4-hour infusion time is usually selected to ensure the achievement of steady-state conditions in plasma and tissues, but was determined not to be sufficient for paclitaxel and vincristine (46). Using the developed model, previously reported $K_{p,uu,brain}$ for paclitaxel (46) and vinorelbine (139) were within two-fold of model-estimated $K_{p,uu,brain}$, which is considered to be acceptable due to potential inter-subject variability. This suggests that all selected MTAs, except eribulin, may have a similar level of unbound partition coefficients across the BBB at steady-state equal to or below 0.03, i.e., 3 % (Table 3). In the case of other CIPN sites, more data on tissue PK after a single dose of the MTA is needed, as each tissue exhibits different PK parameters, including the net influx and efflux and volume of distribution inside the tissue, that could influence the time to reach steady-state (76).

Table 3. Experimentally-derived unbound partition coefficient in the brain at 4 hours ($K_{p,uu,brain,4h}$) for paclitaxel, cabazitaxel, docetaxel, vinorelbine and eribulin, compared to model-estimated unbound brain-to-plasma ratio at the steady-state ($K_{p,uu,brain,ss}$).

Drug	Experimentally-derived $K_{p,uu,brain,4h}$	Estimated time to reach steady-state	Estimated $K_{p,uu,brain,ss}$	Fold differences $(\frac{K_{p,uu,brain,ss}}{K_{p,uu,brain,4h}})$
Paclitaxel	0.006 ± 0.002	40 hours	0.019*	3.2
Cabazitaxel	0.017 ± 0.004	23 hours	0.030	1.8
Docetaxel	0.004 ± 0.001	68.5 hours	0.026	6.5
Vinorelbine	0.008 ± 0.003	11.5 hours	0.014**	1.8
Eribulin	0.0028 ± 0.002	14 hours	0.005	1.8

*The experimentally derived $K_{p,uu,brain,240h}$ was 0.033 ± 0.01 (46). **Literature reported $K_{p,uu,brain}$ was 0.025 (139).

The extent of unbound MTAs' distribution to CIPN sites

Independently of whether MTAs are microtubule stabilizers or destabilizers, all exhibited a greater extent of distribution across endothelial barriers to the PNS tissues compared to the CNS (Fig. 7A). In Papers I and IV-V, at 4-hour determined $K_{p,uu,SN}$ values followed the order as follows: cabazitaxel > docetaxel > vinorelbine > eribulin = paclitaxel, suggesting that the unbound partition coefficient across BNB opposing to the observed CIPN prevalence among

patients, i.e, paclitaxel and cabazitaxel associated with the highest and lowest CIPN risk, respectively (Table 1). However, as previously discussed, MTAs may exhibit different times to reach steady-state in tissues. Thus, the 4-hour data comparison may not be accurate. For example, $K_{p,uu,SN,240h}$ was determined to be 4.5 for paclitaxel (46), while $K_{p,uu,SN,4h}$ was 0.89.

Overall, all MTAs at the 4-hour time point showed $K_{p,uu,tissue}$ to be around unity across BDB and higher than unity at BNB, suggesting that active influx transport is present at the BDB and BNB. Paclitaxel and docetaxel have been confirmed to be substrates of OATP1B1, OATP1B3, and Oatp1b2 (140, 141), and cabazitaxel is a substrate of OATP1B3 (142), while there is little data on vinorelbine and eribulin transporters. Although Oatp1b2 was shown to be expressed in mouse DRG (62), it is not expressed in the human DRG proteome (143), suggesting that there may be other transporters included in MTA transport to the PNS tissues. In contrast to active uptake transporters, there is clear expression of efflux transporters both in the PNS (143) and CNS tissues, and all MTAs are substrates of P-gp (59, 144-147). This is clearly shown by the observed $K_{p,uu,brain,4h}$ being lower than 0.03 for all MTAs. The inhibition of P-gp was shown to increase the risk of CIPN associated with paclitaxel treatment in cancer patients (61), and its lower expression in the PNS was proposed to be one of the reasons for drug accumulation in the PNS (65).

The greatest extent of unbound drug distribution for all MTAs was observed across BSMI, suggesting that the SM can be the most vulnerable across CIPN sites to toxic effects of MTAs. Recently, sarcopenia has been listed as a possible risk factor for CIPN (50). Furthermore, taxanes were shown to affect the microtubule network, glucose homeostasis, and cellular respiration in human primary myotubes in a cell culture model (148), which could lead to clinical implications related to the loss of muscle mass, changes in neuromuscular junctions, and CIPN risk in cancer patients. However, the link between MTAs' exposure in SM and CIPN development is still underexplored.

In contrast to $K_{p,uu,tissue}$, the extent of unbound MTA distribution across cellular barriers was the greatest in the CNS, compared to the PNS tissues. Intracellular exposure of unbound MTAs, governed by the extent of distribution across endothelial and cellular barriers, was the greatest in skeletal muscle, followed by the PNS tissues and the lowest in the CNS. It is not yet clear whether it is mediated through specific transporters or driven by microtubule abundance due to target-mediated drug disposition-like behavior of MTAs (149).

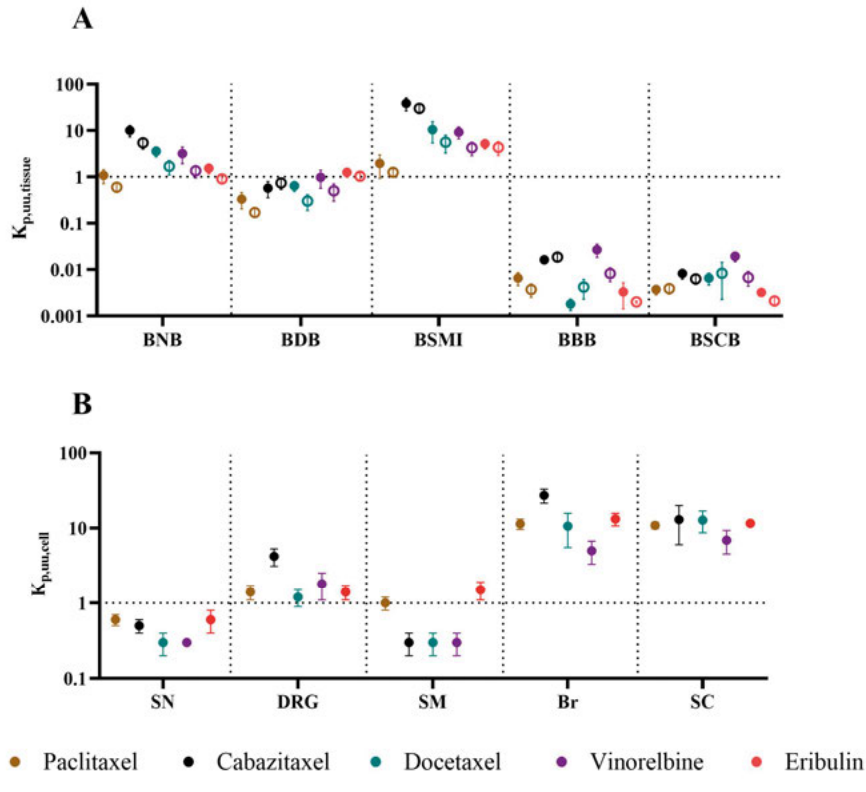

Figure 7. The extent of unbound MTA distribution across endothelial and cellular barriers at CIPN sites. Semilogarithmic dot plots of (A) unbound tissue-to-plasma concentration ratios ($K_{p,uu,tissue}$) and (B) unbound drugs intracellular-to-extracellular concentration ratio ($K_{p,uu,cell}$) in the sciatic nerve (SN), dorsal root ganglia (DRG), skeletal muscle (SM), brain (Br), and spinal cord (SC) of CrEL-paclitaxel (brown), cabazitaxel (black), docetaxel (green), vinorelbine (violet) and eribulin (red) in male (filled) and female (open) Sprague-Dawley rats. The dotted horizontal line indicates a $K_{p,uu,tissue}$ and $K_{p,uu,cell}$ of unity, reflecting passive transport or mutually compensated efflux and influx processes. Data presented as mean with error bars representing standard deviation from the mean. The standard deviations were calculated using the error propagation method (150). Abbreviations: BNB – blood-nerve, BDB – blood-DRG, BBB – blood-brain, BSCB – blood-spinal cord barriers, BSMI – blood-skeletal muscle interface.

Estimation of relative TO

Using generated data on the unbound partition coefficients across endothelial and cellular barriers and literature data on tubulin binding for each MTA, relative TO was estimated in the SN, DRG, SM, and Br, with results described in Paper V. In general, microtubule stabilizers showed higher TO in the SN compared to destabilizers within the same total plasma concentration range

(Fig. 8A). SM and Br were determined to have the highest and lowest TO levels among all investigated MTAs, respectively. Within clinically observed concentrations for each MTA, the estimated TO in the SN and DRG was above 10%, which was previously noted to be required to observe changes in microtubule dynamics after taxane treatment (27). It is not yet clear what level of occupancy could be associated with the neurotoxic effects of MTAs. Due to unbound drug being pharmacologically active, TO was further plotted against unbound plasma concentrations (Fig. 8E-H) and unbound intracellular concentrations (Fig. 8I-L), adjusted to tubulin binding affinity for each MTA. The TO curves became closer to each other when looking at plasma concentrations and overlapped at the same unbound intracellular concentrations in all tissues. Thus, the difference in CIPN prevalence between MTAs could be related to different dosing regimens (Table 1), which could lead to distinct unbound MTA exposure intracellularly. Another important aspect could be the residence time of each MTA bound to tubulin (151), which has been determined to be longer for vincristine than paclitaxel, with times of 518 and 41 seconds, respectively (152, 153).

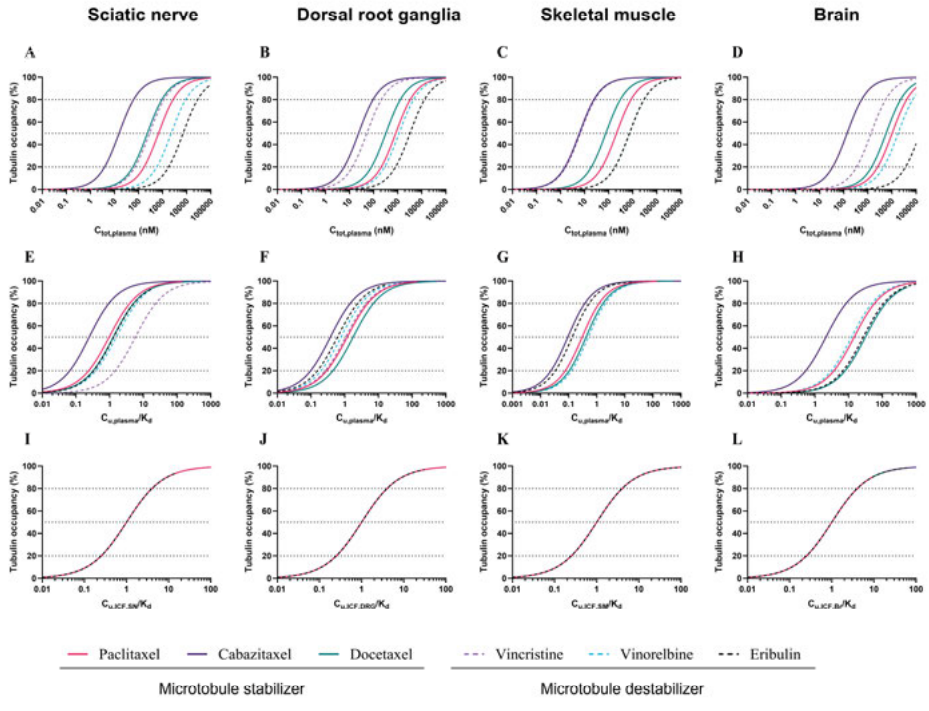

Figure 8. Tubulin occupancy estimation in the sciatic nerve (A, E, I), dorsal root ganglion (B, F, J), skeletal muscle (C, G, K), and brain (D, H, L) for paclitaxel (solid magenta), cabazitaxel (solid purple), docetaxel (solid green), vincristine (dashed purple), vinorelbine (dashed blue), and eribulin (dashed black). Relationship between tubulin occupancy and (A-D) total plasma exposure ($C_{tot,plasma}$, nM), (E-H) unbound rat plasma concentrations ($C_{u,plasma}$, nM) normalized for the dissociation constant (Kd, nM), and (I-L) unbound intracellular rat tissue concentrations ($C_{u,ICF,tissue}$, nM) normalized for the K_d. Occupancies at 20, 50, and 80% are marked with a dotted horizontal line as a visual guide.

Conclusions

This thesis provides novel insights into intra- and extracellular distribution of selected MTAs in CIPN-relevant sites in rodents. Investigated MTAs displayed tissue distribution non-parallel to plasma, thus requiring a tailored study design to investigate the extent of unbound MTA distribution into CIPN sites. In the case of paclitaxel, characterization of intracellular exposure was found to be an essential PK determinant of PIPN development and sNfL kinetics observed in rodents and cancer patients. The developed translational paclitaxel PKPD model can be adapted to accommodate other MTAs' specific characteristics and used as a potential tool for monitoring CIPN in cancer patients.

The generated data in Paper I revealed sex-independent differences in tissue distribution among paclitaxel formulations and a distinctly greater extent of unbound nab- and micellar-paclitaxel distribution across all CIPN-relevant sites, compared to CrEL-paclitaxel. If these formulation-dependent differences translate to humans, they may contribute to variation in clinical CIPN prevalence between paclitaxel formulations. Results from Paper I also suggested that dexamethasone may not alter CrEL-paclitaxel distribution to the tissues, hence unlikely to affect CIPN development. Overall, the findings emphasize that formulation-dependent differences in plasma protein binding, systemic PK, and tissue distribution need to be accounted for in vivo study design and incorporated in mechanistic PKPD model structures exploring PIPN development.

A novel semi-mechanistic paclitaxel PK-NfL model was presented in Paper II, utilizing newly generated experimental data and literature-derived parameters to describe paclitaxel PK and its connection to NfL kinetics. The developed PK model, incorporating experimentally derived tissue-specific $K_{p,uu,tissue}$ and $K_{p,uu,cell}$ values, enabled prediction of unbound intracellular and tubulin-bound paclitaxel exposure in peripheral nerve, DRG, and brain. Model-based analyses indicated that tubulin binding was a key determinant of tissue accumulation. The development of the NfL model was done using a data from a longitudinal preclinical study, quantifying NfL kinetics in serum, CSF, and tissues after a single CrEL-paclitaxel dose, demonstrating a significant increase in sNfL. Integration of the paclitaxel PK and NfL models

enabled development of a novel semi-mechanistic paclitaxel PK–NfL model linking tubulin-bound intracellular paclitaxel exposure to NfL kinetics. The model provides a framework to simulate non-observed scenarios and a basis for translation of preclinical NfL data to clinical applications in PIPN.

In Paper III, population PKPD modelling approaches were successfully employed to establish the link between predicted paclitaxel exposure in plasma and CIPN-relevant sites and reported sNfL concentrations and TNSc in cancer patients shown by model-based simulations describing the data. Two distinct subpopulations were identified, each exhibiting different sNfL kinetics, suggesting the presence of underlying mechanisms yet to be elucidated. ROC analysis indicated that sNfL and TNSc measurements obtained up to week 6 for Subpopulation 2 for patients older than 48 have the highest model-predicted performance, with an AUC of 0.7 for estimating PIPN severity at 12 weeks. The search for other biomarkers remains relevant, as the clinical model analysis presented in this thesis revealed a moderate NfL utility to monitor CIPN development. This suggests a need for more specific biomarkers or a panel consisting of several to establish new CIPN predicting and monitoring strategies.

Eribulin showed an over threefold lower extent of unbound distribution to PNS and CNS tissues than CrEL-paclitaxel in rats (Paper IV). Assuming that a likely similar trend of distribution, i.e., similar $K_{p,uu,tissue}$ and $K_{p,uu,cell}$ values, exists in humans, the lower unbound exposure at CIPN-relevant sites is anticipated. Together with differences in clinical dosing regimens, this may contribute to the lower PIPN burden reported with eribulin relative to paclitaxel. This study also revealed that the assessment of the $K_{p,uu,tissue}$ to CIPN sites requires drug- and tissue-specific experimental design. Eribulin distribution to CIPN sites was determined using a common 4-hour IV infusion approach, while paclitaxel data were obtained after 240 hours of continuous subcutaneous administration via an ALZET pump. These designs reflected predicted differences in the time to steady-state, with eribulin showing nineteen- and three-fold faster attainment of steady-state than paclitaxel in DRG and brain, respectively. Therefore, the violation of the key assumption required for $K_{p,uu,tissue}$ determination, i.e., achievement of steady-state, can become a source of misleading conclusions when comparing the extent of unbound tissue distribution between drugs. Tailored experimental design, including appropriately selected dosing regimen and sampling times, is therefore required to compare distribution kinetics across MTAs at CIPN-relevant sites.

The generated data in Paper V revealed a distinctly greater extent of unbound drug distribution across BNB, BDB, and BSMI compared to BBB and BSCB among all MTAs. Although cellular uptake was more extensive in the

CNS, integration of endothelial and cellular distribution predicted higher intracellular unbound exposure in PNS tissues and skeletal muscle for all three drugs. The higher unbound MTA exposure in peripheral nerves may contribute to greater susceptibility of PNS sites to MTA-induced neurotoxicity compared to CNS. Although the MTAs exhibited broadly similar extent of unbound distribution across CIPN-relevant tissues, their markedly dissimilarities in unbound plasma exposure are expected to produce substantial differences in intracellular exposure. Therefore, systemic unbound exposure, rather than tissue distribution alone, may be an important determinant of the differing CIPN prevalence observed clinically for cabazitaxel, docetaxel, and vinorelbine. The quantitative relationship between MTA-tubulin engagement and CIPN development remains to be established. However, by linking estimated tissue exposure to predicted tubulin occupancy, the work presented here extends the pharmacokinetic comparison toward a pharmacodynamic interpretation and provides a mechanistic basis to understand CIPN development among investigated MTAs.

Future perspectives

This thesis showed the applicability of the CMA-CIPN approach to determine the extent of unbound distribution to CIPN sites of various drugs and drug formulations. This framework can be applied to study novel MTAs, including conventional small molecules and complex modalities, such as ADCs, carrying tubulin-binding payloads. These studies could support early drug-development decisions by identifying drugs with extensive distribution to CIPN sites. They could serve as a component of an integrated risk-assessment strategy combining unbound tissue distribution, intracellular exposure, target engagement, and dosing regimen in relation to CIPN development.

The systemic estimation of the extent of unbound MTA distribution to whole tissue generated in this thesis provides important information about different MTAs exposure at CIPN-relevant sites. However, peripheral nerves and DRG are heterogeneous tissues containing multiple anatomical compartments that may differ in drug exposure. Therefore, future work should focus on increasing spatial resolution of MTA distribution. This may include increasing MALDI-MSI resolution to distinguish smaller structures in the tissue, enhancing the determination of effective CIPN site exposure in the relevant parts of the tissues that are affected during CIPN development. Furthermore, to establish the link between unbound drug concentration and drug effect in a tissue-specific manner, detailed evaluation of tubulin abundance and isoform composition, as well as drug-specific tubulin-binding affinities and binding kinetics, is needed. This may be important if MTAs do not produce equivalent effects at the same total or unbound tissue concentrations and may depend on other tissue- and drug-specific parameters. Altogether, this could help to distinguish drugs that distribute similarly to CIPN sites but differ in their ability to induce neurotoxicity.

The distribution studies in this thesis were performed in healthy animals and therefore established the MTA PK under normal physiological conditions. Future studies should evaluate how tumor presence alters plasma PK, tissue distribution, or the relationship between exposure and CIPN.

Another important aspect is the characterization of transport processes at PNS barriers. The BNB and BDB differ from the CNS barriers, and transporter expression may contribute to the distinct distribution profiles observed in this

thesis. Future work could combine barrier-specific transporter profiling with *in vitro* models of PNS tissues, followed by *in vivo* validation using selective inhibitors or transporter-specific knockout models. This would help to determine whether modulation of these transporters can reduce the extent of distribution and mitigate neurotoxicity of MTAs without compromising antitumor efficacy.

The potential role of skeletal muscle needs to be further established. It is a variable tissue compartment between patients. Thus, clinical analysis combining body composition measurements, plasma PK, blood-based biomarkers, and CIPN assessment could determine whether muscle-related characteristics can partially explain the variability in CIPN prevalence. This may be important in patients with cancer-associated cachexia, sarcopenia, or substantial changes in body composition due to treatment.

The preclinical and clinical findings in this thesis support sNfL as a marker for CIPN development, while also demonstrating the limitations of relying on sNfL alone to predict or monitor CIPN in individual patients. Future studies should evaluate multimarker panels to evaluate the interplay of different biomarkers in predicting and monitoring CIPN development.

The semi-mechanistic model developed in this thesis provides a platform to be extended to incorporate other paclitaxel formulations, MTAs, tissue-specific distribution parameters, tubulin engagement, and biomarkers. These models can be used for *in silico* simulations of alternative dosing regimens, tissue accumulation profiles, and biomarker kinetics. This could guide the selection of clinically relevant MTA concentrations and optimal sampling times for drug and biomarker measurements *in vitro*, *in vivo*, and clinical studies for better understanding of CIPN development.

Popular science summary

Chemotherapy is essential for treating cancer, but it can also damage healthy tissues. Alongside neutropenia, hair loss, and nausea, chemotherapy-induced peripheral neuropathy (CIPN) is a common and sometimes long-lasting adverse event. CIPN manifests as tingling, numbness, burning pain, and weakness in the hands and feet. In severe cases, it can require cancer treatment to be reduced, delayed, or stopped. Effective prevention, monitoring, and treatment options remain limited, making it important to understand how CIPN develops.

This thesis investigated microtubule-targeting agents (MTAs), a widely used class of anticancer drugs. MTAs disrupt cellular structures needed for cancer-cell division, but the same structures are also essential for normal nerve-cell function. Protective barriers regulate drug entry into peripheral nerves, dorsal root ganglia (DRG), brain, spinal cord, and skeletal muscle. However, previous rodent studies suggest that these tissues may be affected during MTA treatment and contribute to CIPN development.

Because nervous system tissues cannot easily be sampled in patients, this work used rodents to study MTA distribution to the nervous system. The results showed that MTAs entered peripheral nerves, DRG, and skeletal muscle more extensively than the brain and spinal cord. This resulted in higher unbound – pharmacologically active – drug exposure in peripheral nervous system tissues linked to CIPN. The findings also suggested that active transport processes may promote drug entry into nerves and DRG, providing possible targets for future prevention and treatment strategies.

Using information generated in preclinical studies, a model was created that can estimate how much of paclitaxel reaches the nervous system tissues in breast cancer patients. To link tissue exposure with neurotoxicity, neurofilament light chain (NfL), a promising blood-based marker of CIPN, was studied. In paclitaxel-treated patients, higher NfL concentrations were associated with more severe neuropathy symptoms. However, simulations showed that NfL is not accurate enough to predict CIPN development for every individual. This suggests a need for further research for more selective biomarkers for CIPN prediction in cancer patients.

Overall, this work improves understanding of MTA distribution and why peripheral nerves are especially vulnerable to chemotherapy. It also shows

how preclinical studies and mathematical modelling can address questions that cannot be directly studied in patients, supporting the development of safer chemotherapy, earlier detection of neurotoxicity, and improved prevention and treatment of CIPN.

Acknowledgements

The work presented in this thesis was mostly conducted in the Department of Pharmacy at Uppsala University. NfL quantification was done at the Unit of Affinity Proteomics at SciLifeLab, Stockholm. I want to express my deepest gratitude to Vilnius University for financial support during the whole period of my PhD journey. I want to acknowledge financial support for research from the Swedish Research Council (Vetenskapsrådet, VR 2018-05973 and 2022-01098), the Innovative Medicines Initiative to Joint Undertaking project NeuroDeRisk (grant 821528), and the Swedish Cancer Society (funding number 23 2921 Pj and 25 4902 Pj). I acknowledge the support provided by the Swedish National Infrastructure for Computing (SNIC) and the National Academic Infrastructure for Supercomputing in Sweden (NAISS) at Uppsala University, partially funded by the Swedish Research Council through grant agreement no. 2018-05973 and 2022-06725 for supporting mathematical modeling work.

This thesis was originally written by me as a doctoral student. Generative AI has been used for linguistic changes and additional literature search and analysis using the Perplexity tool. This usage follows the guidelines for the use of generative AI in the faculty's general study syllabus for doctoral education.

I'm thankful to the Swedish Academy of Pharmaceutical Sciences (Apotekarsocieteten), ULLA European University Consortium for Pharmaceutical Sciences, Anna-Maria Lundin's Foundation, and The Nordic Pharmaceutical Translation and Innovation (NordicPharmaTrain) for granting travel grants for participation in scientific meetings and conferences. Additionally, thank you to the Lithuanian Academy of Sciences and BrightFocus Foundation for acknowledging my work presented at the conferences.

This journey of learning and discovery would have been impossible without the support of everyone, from long before it started until the very last minute. The time, guidance, and kindness you gave me are gifts I will always treasure.

Ačiū to my main supervisor, Irena Loryan. I'm grateful for accepting me as part of your team and for pouring all your knowledge and insights into every project. Thank you for all the time spent in discussions and the thousands of valuable comments to help me climb the ladder of science. Thank you for your

constant reminders to build up the confidence in saying yes and no to hundreds of opportunities you have opened doors to explore during this journey.

Ačiū to my co-supervisor, Lena Friberg. I'm honored to be introduced by you to the world of pharmacometrics! Thank you for sharing your knowledge on how to approach mathematical modeling and highlight its clinical applications.

Ačiū to my co-supervisor, Margareta Hammarlund-Udenaes. Thank you for showing me the tools to balance scientific and personal life and that it is fine to have a busy mind. Thank you for sharing your immense expertise in pharmacokinetics and all your valuable comments. Thank you for helping me to find a place in Sweden that I can call my second home.

Ačiū to my co-supervisor, Stina Syvänen. Thank you for always being there to discuss research questions, asking details that make my brain gears rotate a little bit more. Thank you for being an inspiring example of how to sail across the scientific community and keep updated with the research.

Ačiū to my co-supervisor, Jolanta Gulbinovič. Dėkoju, kad buvote inkaru už namų ribų, kuomet kildavo klausimas ar judu teisinga linkme. Ačiū už dalinimąsi patirtimi ir įžvalgomis kaip surasti savo vietą tarp švediško ir lietuviško mokslo.

Ačiū to the members and visitors of the Translational PKPD group. Ačiū, Aghavni, for being my partner in crime since day one. I treasure every memory of our adventures. Ačiū, Frida, for being an inspiring example of a PhD student and showing the Swedish way to take care of yourself. Ačiū, Canan, for that Turkish coffee and for sharing important questions to consider while planning the scientific journey. Ačiū, Jessica, for your patience and lessons on all laboratory work, thank you for your great support!

Ačiū to all collaborators and co-authors. Thank you, Eman, for being a huge part of my journey, it was a pleasure to learn and work with you! Thank you Yang, Lorenzo, David, Jérôme, Diethilde, Gautier, Olivier, Nathalie, Franck, Muhamed, Roser, Jordi, Andreas, and Haralabos, for sharing their insights on preclinical and clinical paclitaxel and NfL data. Thank you, Claudia, Matilda, and Maryam, for sharing your expertise and providing support for NfL analysis. I'm grateful for the opportunity to join and learn how things are done in SciLifeLabs.

Nuoširdžiausias ačiū to Indrė Trečiokienė už didžiausią palaikymą prieš pradedant šią doktorantūros kelionę ir už tai, kad padėjote galimybę paversti tikrove. Ačiū, kad parodėte kaip drąsiai ir sistemingai spręsti sudėtingus klausimus bei atkakliai siekti rezultatų. Ačiū Kristinai Garuolienei už suteiktus kelius įsitraukti į mokslines veiklas Lietuvoje. Ačiū Godai Elizabetai Vaitkevičienei, už bendradarbiavimą ir atvertas galimybes tolimesniems darbams.

Ačiū to my master's students Rojita, Joseph, and Fatema for all the fun times in the laboratory and great discussions, wondering what's happening in the results sheets. Ačiū to the pharmacy students back at Vilnius University for sharing great questions and the opportunity to learn together.

Ačiū to all PhD students I have met during these years. Thank you for sharing your ideas, research questions, and fun times through various occasions.

Ačiū to all colleagues at the department for making the Department of Pharmacy feel like home. Thank you for all the learning opportunities, the wonderful Fika and after-work activities.

Ačiū to my dearest friends back in Lithuania for keeping up the contact while I'm far away, and for catching up with good times during those short times back in Lithuania.

Ačiū savo mamai ir tėčiui už nuolatinį rūpestį ir milijonus skambučių, kuomet pradingstu tarp visų darbų. Ačiū už jūsų ištvermę, meilę ir laiką kartu. Ačiū, myliu ir bučiuoju.

Jūs buvote šalia—
todėl ir tolimas kelias
tapo įveikiamas.

Milda
Upsala, Švedija
Spalis, 2026

References

1. World Health Organization. Global status report on cancer 2026: the future we choose together. Geneva: World Health Organization. ISBN: 978-92-4-012397-7. Available from: https://www.who.int/publications/i/item/9789240123977. Accessed on the 21st of August, 2026 2026:280 p.
2. Falzone L, Salomone S, Libra M. Evolution of Cancer Pharmacological Treatments at the Turn of the Third Millennium. Frontiers in pharmacology. 2018;9:1300.
3. Al-Karmalawy AA, Eissa ME, Ashour NA, Yousef TA, Al Khatib AO, Hawas SS. Medicinal chemistry perspectives on anticancer drug design based on clinical applications (2015–2025). RSC Advances. 2025;15(43):36441-71.
4. Hota A, Mandal BK. Unveiling the hidden harms: a review on the deeper exploration of side effects of oncotherapy. Medical Oncology. 2025;43(2):75.
5. Jordan B, Margulies A, Cardoso F, Cavaletti G, Haugnes HS, Jahn P, et al. Systemic anticancer therapy-induced peripheral and central neurotoxicity: ESMO-EONS-EANO Clinical Practice Guidelines for diagnosis, prevention, treatment and follow-up. Annals of oncology : official journal of the European Society for Medical Oncology. 2020;31(10):1306-19.
6. Zhang B, Lau LY, Wu Z, Chen Y. Chemotherapy induced neurotoxicity in cancer survivors assessed through a dual database bibliometric analysis from 2005 to 2025. Discover Oncology. 2025;16(1):1961.
7. Zedan AH, Vilholm OJ. Chemotherapy-Induced Polyneuropathy: Major Agents and Assessment by Questionnaires. 2014;115(2):193-200.
8. Seretny M, Currie GL, Sena ES, Ramnarine S, Grant R, MacLeod MR, et al. Incidence, prevalence, and predictors of chemotherapy-induced peripheral neuropathy: A systematic review and meta-analysis. Pain. 2014;155(12): 2461-70.
9. Kishimoto S, Oshima N, Rinker M, Krishna MC, Takebe N. Identification of high-risk drugs related to chemotherapy-induced peripheral neuropathy in Cancer Therapy Evaluation Program-sponsored phase I trials. European journal of cancer (Oxford, England : 1990). 2019;115:111-9.
10. Tanabe Y, Hashimoto K, Shimizu C, Hirakawa A, Harano K, Yunokawa M, et al. Paclitaxel-induced peripheral neuropathy in patients receiving adjuvant chemotherapy for breast cancer. Int J Clin Oncol. 2013;18(1):132-8.
11. Molassiotis A, Cheng HL, Leung KT, Li YC, Wong KH, Au JSK, et al. Risk factors for chemotherapy-induced peripheral neuropathy in patients receiving taxane- and platinum-based chemotherapy. Brain and behavior. 2019;9(6):e01312.
12. Mielke S, Sparreboom A, Steinberg SM, Gelderblom H, Unger C, Behringer D, et al. Association of Paclitaxel pharmacokinetics with the development of peripheral neuropathy in patients with advanced cancer. Clinical cancer research : an official journal of the American Association for Cancer Research. 2005;11(13):4843-50.

13. Seidman AD, Berry D, Cirrincione C, Harris L, Muss H, Marcom PK, et al. Randomized Phase III Trial of Weekly Compared With Every-3-Weeks Paclitaxel for Metastatic Breast Cancer, With Trastuzumab for all HER-2 Overexpressors and Random Assignment to Trastuzumab or Not in HER-2 Nonoverexpressors: Final Results of Cancer and Leukemia Group B Protocol 9840. 2008;26(10):1642-9.
14. Huang T-C, Campbell TC. Comparison of weekly versus every 3 weeks paclitaxel in the treatment of advanced solid tumors: A meta-analysis. Cancer Treatment Reviews. 2012;38(6):613-7.
15. Timmins HC, Li T, Trinh T, Kiernan MC, Harrison M, Boyle F, et al. Weekly Paclitaxel-Induced Neurotoxicity in Breast Cancer: Outcomes and Dose Response. Oncologist. 2021;26(5):366-74.
16. Was H, Borkowska A, Bagues A, Tu L, Liu JYH, Lu Z, et al. Mechanisms of Chemotherapy-Induced Neurotoxicity. Frontiers in Pharmacology. 2022;13:750507.
17. Dougherty PM, Cata JP, Cordella JV, Burton A, Weng HR. Taxol-induced sensory disturbance is characterized by preferential impairment of myelinated fiber function in cancer patients. Pain. 2004;109(1-2):132-42.
18. Miyashita M. Chemotherapy-related cognitive impairment: What we need to know and what we can do. Asia-Pacific journal of oncology nursing. 2024;11(1):100334.
19. Bao T, Basal C, Seluzicki C, Li SQ, Seidman AD, Mao JJ. Long-term chemotherapy-induced peripheral neuropathy among breast cancer survivors: prevalence, risk factors, and fall risk. Breast cancer research and treatment. 2016;159(2):327-33.
20. Smith E. Current Methods for the Assessment and Management of Taxane-Related Neuropathy. Clinical journal of oncology nursing. 2013;17:22-34.
21. Trotti A, Byhardt R, Stetz J, Gwede C, Corn B, Fu K, et al. Common toxicity criteria: version 2.0. an improved reference for grading the acute effects of cancer treatment: impact on radiotherapy. International journal of radiation oncology, biology, physics. 2000;47(1):13-47.
22. Cornblath DR, Chaudhry V, Carter K, Lee D, Seysedadr M, Miernicki M, et al. Total neuropathy score. Neurology. 1999;53(8):1660-.
23. Cavaletti G, Frigeni B, Lanzani F, Piatti M, Rota S, Briani C, et al. The Total Neuropathy Score as an assessment tool for grading the course of chemotherapy-induced peripheral neurotoxicity: comparison with the National Cancer Institute-Common Toxicity Scale. Journal of the peripheral nervous system : JPNS. 2007;12(3):210-5.
24. Janke C, Magiera MM. The tubulin code and its role in controlling microtubule properties and functions. Nature reviews Molecular cell biology. 2020;21(6):307-26.
25. Kumari A, Panda D. Monitoring the Disruptive Effects of Tubulin-Binding Agents on Cellular Microtubules. Methods in molecular biology (Clifton, NJ). 2022;2430:431-48.
26. Wang X, Gigant B, Zheng X, Chen Q. Microtubule-targeting agents for cancer treatment: Seven binding sites and three strategies. 2023;2(3):e46.
27. Pineda JJ, Miller MA, Song Y, Kuhn H, Mikula H, Tallapragada N, et al. Site occupancy calibration of taxane pharmacology in live cells and tissues. Proceedings of the National Academy of Sciences of the United States of America. 2018;115(48):E11406-e14.

28. Burgess J, Ferdousi M, Gosal D, Boon C, Matsumoto K, Marshall A, et al. Chemotherapy-Induced Peripheral Neuropathy: Epidemiology, Pathomechanisms and Treatment. Oncol Ther. 2021;9(2):385-450.
29. Calligaris D, Verdier-Pinard P, Devred F, Villard C, Braguer D, Lafitte D. Microtubule targeting agents: From biophysics to proteomics. Cellular and molecular life sciences : CMLS. 2010;67:1089-104.
30. Winer EP, Berry DA, Woolf S, Duggan D, Kornblith A, Harris LN, et al. Failure of higher-dose paclitaxel to improve outcome in patients with metastatic breast cancer: cancer and leukemia group B trial 9342. Journal of clinical oncology : official journal of the American Society of Clinical Oncology. 2004;22(11):2061-8.
31. de Bono JS, Oudard S, Ozguroglu M, Hansen S, Machiels JP, Kocak I, et al. Prednisone plus cabazitaxel or mitoxantrone for metastatic castration-resistant prostate cancer progressing after docetaxel treatment: a randomised open-label trial. Lancet (London, England). 2010;376(9747):1147-54.
32. Valero V, Forbes J, Pegram MD, Pienkowski T, Eiermann W, von Minckwitz G, et al. Multicenter phase III randomized trial comparing docetaxel and trastuzumab with docetaxel, carboplatin, and trastuzumab as first-line chemotherapy for patients with HER2-gene-amplified metastatic breast cancer (BCIRG 007 study): two highly active therapeutic regimens. Journal of clinical oncology : official journal of the American Society of Clinical Oncology. 2011;29(2):149-56.
33. Stubblefield MD, Burstein HJ, Burton AW, Custodio CM, Deng GE, Ho M, et al. NCCN task force report: management of neuropathy in cancer. Journal of the National Comprehensive Cancer Network : JNCCN. 2009;7 Suppl 5:S1-S26; quiz S7-8.
34. Cienkusz M, Drabko K. The incidence and clinical spectrum of vincristine- induced peripheral neuropathy in patients with acute lymphoblastic leukemia- a prospective study of twenty-nine cases. Acta Haematologica Polonica. 2024;55(1):42-7.
35. Smith EML, Kuisell C, Cho Y, Kanzawa-Lee GA, Gilchrist LS, Park SB, et al. Characteristics and patterns of pediatric chemotherapy-induced peripheral neuropathy: A systematic review. Cancer treatment and research communications. 2021;28:100420.
36. Tazi A, Lorillon G, Haroche J, Neel A, Dominique S, Aouba A, et al. Vinblastine chemotherapy in adult patients with langerhans cell histiocytosis: a multicenter retrospective study. Orphanet journal of rare diseases. 2017;12(1):95.
37. Andersson M, López-Vega JM, Petit T, Zamagni C, Easton V, Kamber J, et al. Efficacy and Safety of Pertuzumab and Trastuzumab Administered in a Single Infusion Bag, Followed by Vinorelbine: VELVET Cohort 2 Final Results. The oncologist. 2017;22(10):1160-8.
38. Eigentler TK, Radny P, Hauschild A, Gutzmer R, Linse R, Pföhler C, et al. Adjuvant treatment with vindesine in comparison to observation alone in patients with metastasized melanoma after complete metastasectomy: a randomized multicenter trial of the German Dermatologic Cooperative Oncology Group. Melanoma Research. 2008;18(5).
39. Holmsten K, Jensen NV, Mouritsen LS, Jonsson E, Mellnert C, Agerbæk M, et al. Vinflunine/gemcitabine versus carboplatin/gemcitabine as first-line treatment in cisplatin-ineligible patients with advanced urothelial carcinoma: A randomised phase II trial (VINGEM). European journal of cancer (Oxford, England : 1990). 2020;127:173-82.

40. Schmidt M, Hesse T, Hoffmann O, Heinrich BJ, Park-Simon T-W, Grischke E-M, et al. Eribulin-Induced Peripheral Neuropathy in Locally Advanced or Metastatic Breast Cancer: Final Analysis of the Prospective Cohort IRENE Study. Cancers. 2025;17(3):457.
41. Andreu JM, Barasoain I. The Interaction of Baccatin III with the Taxol Binding Site of Microtubules Determined by a Homogeneous Assay with Fluorescent Taxoid. Biochemistry. 2001;40(40):11975-84.
42. Smiyun G, Azarenko O, Miller H, Rifkind A, LaPointe NE, Wilson L, et al. βIII-tubulin enhances efficacy of cabazitaxel as compared with docetaxel. Cancer Chemotherapy and Pharmacology. 2017;80(1):151-64.
43. Lobert S, Ingram JW, Hill BT, Correia JJ. A comparison of thermodynamic parameters for vinorelbine- and vinflunine-induced tubulin self-association by sedimentation velocity. Molecular pharmacology. 1998;53(5):908-15.
44. Smith JA, Wilson L, Azarenko O, Zhu X, Lewis BM, Littlefield BA, et al. Eribulin binds at microtubule ends to a single site on tubulin to suppress dynamic instability. Biochemistry. 2010;49(6):1331-7.
45. Peters CM, Jimenez-Andrade JM, Kuskowski MA, Ghilardi JR, Mantyh PW. An evolving cellular pathology occurs in dorsal root ganglia, peripheral nerve and spinal cord following intravenous administration of paclitaxel in the rat. Brain research. 2007;1168:46-59.
46. Hu Y, Girdenyté M, Roest L, Liukkonen I, Siskou M, Bällgren F, et al. Analysis of the contributing role of drug transport across biological barriers in the development and treatment of chemotherapy-induced peripheral neuropathy. Fluids and barriers of the CNS. 2024;21(1):13.
47. Wozniak KM, Vornov JJ, Wu Y, Nomoto K, Littlefield BA, DesJardins C, et al. Sustained Accumulation of Microtubule-Binding Chemotherapy Drugs in the Peripheral Nervous System: Correlations with Time Course and Neurotoxic Severity. Cancer research. 2016;76(11):3332-9.
48. Cherchi L, Zippo AG, Fantoni L, Carozzi VA, Marmiroli PJRitN. From peripheral neurotoxicity to central dysfunction: linking neuropathic pain and cognition in chemotherapy-induced peripheral neuropathy. 2026;37:553 - 76.
49. Omran M, Belcher EK, Mohile NA, Kesler SR, Janelsins MC, Hohmann AG, et al. Review of the Role of the Brain in Chemotherapy-Induced Peripheral Neuropathy. Frontiers in molecular biosciences. 2021;8:693133.
50. Velasco R, Besora S, Bellver M, Peiró I, Marco C, Domingo-Domenech E, et al. Sarcopenia in Patients With Cancer and Its Association With Chemotherapy-Induced Peripheral Neurotoxicity. Neurology. 2026;106(10):e214987.
51. Jiang Y, Guo J, Zhao J, Chen F, Hou J, Li X, et al. Exploratory analysis of the association between body composition albumin-bound paclitaxel induced peripheral neuropathy. Frontiers in pharmacology. 2026;17:1644444.
52. Reinhold AK, Rittner HL. Characteristics of the nerve barrier and the blood dorsal root ganglion barrier in health and disease. Experimental neurology. 2020;327:113244.
53. Jimenez-Andrade JM, Herrera MB, Ghilardi JR, Vardanyan M, Melemedjian OK, Mantyh PW. Vascularization of the dorsal root ganglia and peripheral nerve of the mouse: implications for chemical-induced peripheral sensory neuropathies. Molecular pain. 2008;4:10.
54. Knauer MJ, Urquhart BL, Meyer zu Schwabedissen HE, Schwarz UI, Lemke CJ, Leake BF, et al. Human Skeletal Muscle Drug Transporters Determine Local Exposure and Toxicity of Statins. Circulation Research. 2010;106(2):297-306.

55. Abbott NJ, Patabendige AAK, Dolman DEM, Yusof SR, Begley DJ. Structure and function of the blood–brain barrier. Neurobiology of Disease. 2010;37(1):13-25.
56. Malong L, Napoli I, Casal G, White IJ, Stierli S, Vaughan A, et al. Characterization of the structure and control of the blood-nerve barrier identifies avenues for therapeutic delivery. Developmental Cell. 2023;58(3):174-91.e8.
57. Ubogu EE. Biology of the human blood-nerve barrier in health and disease. Experimental neurology. 2020;328:113272.
58. Hammarlund-Udenaes M, Fridén M, Syvänen S, Gupta A. On The Rate and Extent of Drug Delivery to the Brain. Pharmaceutical Research. 2008;25(8):1737-50.
59. Fellner S, Bauer B, Miller DS, Schaffrik M, Fankhänel M, Spruss T, et al. Transport of paclitaxel (Taxol) across the blood-brain barrier in vitro and in vivo. The Journal of clinical investigation. 2002;110(9):1309-18.
60. Wang F, Zhou F, Kruh GD, Gallo JM. Influence of blood-brain barrier efflux pumps on the distribution of vincristine in brain and brain tumors. Neuro-Oncology. 2010;12(10):1043-9.
61. Stage TB, Mortensen C, Khalaf S, Steffensen V, Hammer HS, Xiong C, et al. P-Glycoprotein Inhibition Exacerbates Paclitaxel Neurotoxicity in Neurons and Patients With Cancer. Clinical pharmacology and therapeutics. 2020;108(3):671-80.
62. Leblanc AF, Sprowl JA, Alberti P, Chiorazzi A, Arnold WD, Gibson AA, et al. OATP1B2 deficiency protects against paclitaxel-induced neurotoxicity. The Journal of clinical investigation. 2018;128(2):816-25.
63. Svoboda M, Wlcek K, Taferner B, Hering S, Stieger B, Tong D, et al. Expression of organic anion-transporting polypeptides 1B1 and 1B3 in ovarian cancer cells: relevance for paclitaxel transport. Biomedicine & pharmacotherapy = Biomedecine & pharmacotherapie. 2011;65(6):417-26.
64. Kobayashi Y, Ohshiro N, Sakai R, Ohbayashi M, Kohyama N, Yamamoto T. Transport mechanism and substrate specificity of human organic anion transporter 2 (hOat2 [SLC22A7]). The Journal of pharmacy and pharmacology. 2005;57(5):573-8.
65. Stage TB, Hu S, Sparreboom A, Kroetz DL. Role for Drug Transporters in Chemotherapy-Induced Peripheral Neuropathy. Clinical and translational science. 2021;14(2):460-7.
66. Lee J, Choi M-K, Song I-S. Recent paclitaxel formulation strategies: expanding the therapeutic index by addressing biopharmaceutical and toxicity limitations. Archives of Pharmacal Research. 2026;49(4):500-33.
67. Gelderblom H, Verweij J, Nooter K, Sparreboom A. Cremophor EL: the drawbacks and advantages of vehicle selection for drug formulation. European journal of cancer (Oxford, England : 1990). 2001;37(13):1590-8.
68. Park JH, Kim YJ, Kwon KE, Lee SG, Lee BK, Lee HJ. Effects of formulation on pharmacokinetics of docetaxel in rats. Journal of Pharmaceutical Investigation. 2012;42(1):51-5.
69. Li F, Zhang H, He M, Liao J, Chen N, Li Y, et al. Different Nanoformulations Alter the Tissue Distribution of Paclitaxel, Which Aligns with Reported Distinct Efficacy and Safety Profiles. Mol Pharm. 2018;15(10):4505-16.
70. Liu M, Liu S, Yang L, Wang S. Comparison between nab-paclitaxel and solvent-based taxanes as neoadjuvant therapy in breast cancer: a systematic review and meta-analysis. BMC Cancer. 2021;21(1):118.

71. Klecker RW, Jamis-Dow CA, Egorin MJ, Erkmen K, Parker RJ, Stevens R, et al. Effect of cimetidine, probenecid, and ketoconazole on the distribution, biliary secretion, and metabolism of [3H]taxol in the Sprague-Dawley rat. Drug Metab Dispos. 1994;22(2):254-8.
72. Vrignaud P, Semiond D, Benning V, Beys E, Bouchard H, Gupta S. Preclinical profile of cabazitaxel. Drug design, development and therapy. 2014;8:1851-67.
73. Summerfield SG, Yates JWT, Fairman DA. Free Drug Theory - No Longer Just a Hypothesis? Pharm Res. 2022;39(2):213-22.
74. Fridén M, Gupta A, Antonsson M, Bredberg U, Hammarlund-Udenaes M. In vitro methods for estimating unbound drug concentrations in the brain interstitial and intracellular fluids. Drug metabolism and disposition: the biological fate of chemicals. 2007;35(9):1711-9.
75. Loryan I, Sinha V, Mackie C, Van Peer A, Drinkenburg W, Vermeulen A, et al. Mechanistic understanding of brain drug disposition to optimize the selection of potential neurotherapeutics in drug discovery. Pharm Res. 2014;31(8):2203-19.
76. Syvänen S, Xie R, Sahin S, Hammarlund-Udenaes M. Pharmacokinetic Consequences of Active Drug Efflux at the Blood–Brain Barrier. Pharm Res. 2006;23(4):705-17.
77. Fridén M, Ducrozet F, Middleton B, Antonsson M, Bredberg U, Hammarlund-Udenaes M. Development of a high-throughput brain slice method for studying drug distribution in the central nervous system. Drug metabolism and disposition: the biological fate of chemicals. 2009;37(6):1226-33.
78. Hammarlund-Udenaes M DLE, Thorne R. Drug Delivery to the Brain: Physiological Concepts, Methodologies and Approaches. 2nd edition. 2022.
79. Fridén M, Bergström F, Wan H, Rehngren M, Ahlin G, Hammarlund-Udenaes M, et al. Measurement of Unbound Drug Exposure in Brain: Modeling of pH Partitioning Explains Diverging Results between the Brain Slice and Brain Homogenate Methods. Drug Metab Dispos. 2011;39(3):353-62.
80. Kalvass JC, Maurer TS. Influence of nonspecific brain and plasma binding on CNS exposure: implications for rational drug discovery. Biopharmaceutics & drug disposition. 2002;23(8):327-38.
81. Loryan I, Sinha V, Mackie C, Van Peer A, Drinkenburg W, Vermeulen A, et al. Mechanistic Understanding of Brain Drug Disposition to Optimize the Selection of Potential Neurotherapeutics in Drug Discovery. Pharm Res. 2014;31(8):2203-19.
82. Loryan I, Fridén M, Hammarlund-Udenaes MJF, CNS Bot. The brain slice method for studying drug distribution in the CNS. Fluids and barriers of the CNS. 2013;10:6 -
83. Rzagalinski I, Volmer DA. Quantification of low molecular weight compounds by MALDI imaging mass spectrometry – A tutorial review. Biochimica et Biophysica Acta (BBA) - Proteins and Proteomics. 2017;1865(7):726-39.
84. Guo S, Li K, Chen Y, Li B. Unraveling the drug distribution in brain enabled by MALDI MS imaging with laser-assisted chemical transfer. Acta pharmaceutica Sinica B. 2022;12(4):2120-6.
85. Demuytere J, Carlier C, Van de Sande L, Hoorens A, De Clercq K, Giordano S, et al. Preclinical Activity of Two Paclitaxel Nanoparticle Formulations After Intraperitoneal Administration in Ovarian Cancer Murine Xenografts. International journal of nanomedicine. 2024;19:429-40.
86. Körber A, Anthony IGM, Heeren RMA. Mass Spectrometry Imaging. Analytical chemistry. 2025;97(29):15517-49.

87. Kolluru C, Todd A, Upadhye AR, Liu Y, Berezin MY, Fereidouni F, et al. Imaging peripheral nerve micro-anatomy with MUSE, 2D and 3D approaches. Scientific reports. 2022;12(1):10205.
88. Carozzi VA, Salio C, Rodriguez-Menendez V, Ciglieri E, Ferrini F. 2D vs 3D morphological analysis of dorsal root ganglia in health and painful neuropathy. European journal of histochemistry : EJH. 2021;65(s1).
89. Hammarlund-Udenaes M. Microdialysis as an Important Technique in Systems Pharmacology—a Historical and Methodological Review. AAPS J. 2017;19(5):1294-303.
90. Chaurasia CS, Müller M, Bashaw ED, Benfeldt E, Bolinder J, Bullock R, et al. AAPS-FDA Workshop White Paper: Microdialysis Principles, Application, and Regulatory Perspectives. 2007;47(5):589-603.
91. Loos WJ, Zamboni WC, Engels FK, de Bruijn P, Lam MH, de Wit R, et al. Pitfalls of the application of microdialysis in clinical oncology: Controversial findings with docetaxel. Journal of Pharmaceutical and Biomedical Analysis. 2007;45(2):288-94.
92. Eroglu Z, Synold T, Badie B, Liu A, Chowdhury A, Kilpatrick J, et al. An intracerebral microdialysis study to determine the neuropharmacokinetics of eribulin in patients with metastatic or primary brain tumors. Cancer chemotherapy and pharmacology. 2024;94(6):807-13.
93. Rodwin RL, Siddiq NZ, Ehrlich BE, Lustberg MB. Biomarkers of Chemotherapy-Induced Peripheral Neuropathy: Current Status and Future Directions. Front Pain Res (Lausanne). 2022;3:864910.
94. Keddie S, Smyth D, Keh RYS, Chou MKL, Grant D, Surana S, et al. Peripherin is a biomarker of axonal damage in peripheral nervous system disease. Brain : a journal of neurology. 2023;146(11):4562-73.
95. Yuan A, Rao MV, Veeranna, Nixon RA. Neurofilaments and Neurofilament Proteins in Health and Disease. Cold Spring Harbor perspectives in biology. 2017;9(4).
96. Loeffler T, Schilcher I, Flunkert S, Hutter-Paier B. Neurofilament-Light Chain as Biomarker of Neurodegenerative and Rare Diseases With High Translational Value. Front Neurosci. 2020;14:579.
97. Sano T, Masuda Y, Yasuno H, Shinozawa T, Watanabe T, Kakehi M. Blood Neurofilament Light Chain as a Potential Biomarker for Central and Peripheral Nervous Toxicity in Rats. Toxicological Sciences. 2021;185(1):10-8.
98. Mortensen C, Steffensen KD, Simonsen E, Herskind K, Madsen JS, Olsen DA, et al. Neurofilament light chain as a biomarker of axonal damage in sensory neurons and paclitaxel-induced peripheral neuropathy in patients with ovarian cancer. Pain. 2023;164(7):1502-11.
99. Pontoppidan PEL, Vase CB, Mortensen C, Andres-Jensen L, Olsen DA, Madsen JS, et al. Neurofilament light chain as in vitro and clinical biomarker of vincristine-induced peripheral neuropathy. British Journal of Clinical Pharmacology. 2026;92(9):3180-90.
100. Meregalli C, Fumagalli G, Alberti P, Canta A, Carozzi VA, Chiorazzi A, et al. Neurofilament light chain as disease biomarker in a rodent model of chemotherapy induced peripheral neuropathy. Experimental Neurology. 2018;307:129-32.
101. Meregalli C, Fumagalli G, Alberti P, Canta A, Chiorazzi A, Monza L, et al. Neurofilament light chain: a specific serum biomarker of axonal damage severity in rat models of Chemotherapy-Induced Peripheral Neurotoxicity. Archives of toxicology. 2020;94(7):2517-22.
102. Balayssac D, Durif J, Lambert C, Dalbos C, Chapuy E, Etienne M, et al. Exploring Serum Biomarkers for Neuropathic Pain in Rat Models of Chemotherapy-

Induced Peripheral Neuropathy: A Comparative Pilot Study with Oxaliplatin, Paclitaxel, Bortezomib, and Vincristine. Toxics. 2023;11(12).
103. Karteri S, Bruna J, Argyriou AA, Mariotto S, Velasco R, Alemany M, et al. Prospectively assessing serum neurofilament light chain levels as a biomarker of paclitaxel-induced peripheral neurotoxicity in breast cancer patients. Journal of the peripheral nervous system : JPNS. 2022;27(2):166-74.
104. Smyth D, Keh RYS, Keddie S, Chou M, Hart M, Chapman M, et al. Prospective assessment of serum neurofilament light chain in platinum-induced and taxane-induced peripheral neuropathy. BMJ neurology open. 2026;8(1):e001312.
105. Alberti P, Faithfull S, Argyriou AA, Balayssac D, Hertz DL, Lustberg M, et al. Serum neurofilament light chain (sNFL) as a predictive biomarker for Chemotherapy-induced peripheral neurotoxicity (CIPN): consideration of current evidence, validation steps, and barriers to CIPN biomarker implementation in clinical practice-a narrative review. Supportive care in cancer : official journal of the Multinational Association of Supportive Care in Cancer. 2026;34(6).
106. Liu H, Ibrahim EIK, Centanni M, Sarr C, Venkatakrishnan K, Friberg LE. Integrated modeling of biomarkers, survival and safety in clinical oncology drug development. Advanced drug delivery reviews. 2025;216:115476.
107. Henningsson A, Karlsson MO, Viganò L, Gianni L, Verweij J, Sparreboom A. Mechanism-based pharmacokinetic model for paclitaxel. Journal of clinical oncology : official journal of the American Society of Clinical Oncology. 2001;19(20):4065-73.
108. Henningsson A, Sparreboom A, Sandström M, Freijs A, Larsson R, Bergh J, et al. Population pharmacokinetic modelling of unbound and total plasma concentrations of paclitaxel in cancer patients. European journal of cancer (Oxford, England : 1990). 2003;39(8):1105-14.
109. Chen N, Li Y, Ye Y, Palmisano M, Chopra R, Zhou S. Pharmacokinetics and pharmacodynamics of nab-paclitaxel in patients with solid tumors: disposition kinetics and pharmacology distinct from solvent-based paclitaxel. J Clin Pharmacol. 2014;54(10):1097-107.
110. Kraff S, Nieuweboer AJM, Mathijssen RHJ, Baty F, de Graan A-J, van Schaik RHN, et al. Pharmacokinetically based dosing of weekly paclitaxel to reduce drug-related neurotoxicity based on a single sample strategy. Cancer Chemotherapy and Pharmacology. 2015;75(5):975-83.
111. Sun Y, Pai MP, Henry NL, Hertz DL. Pharmacokinetic-Pharmacodynamic Model of Paclitaxel-Induced Peripheral Neuropathy. Clinical and translational science. 2025;18(11):e70404.
112. Mehrotra S, Sharma MR, Gray E, Wu K, Barry WT, Hudis C, et al. Kinetic-Pharmacodynamic Model of Chemotherapy-Induced Peripheral Neuropathy in Patients with Metastatic Breast Cancer Treated with Paclitaxel, Nab-Paclitaxel, or Ixabepilone: CALGB 40502 (Alliance). Aaps j. 2017;19(5):1411-23.
113. Zhang J, Zhou F, Qi H, Ni H, Hu Q, Zhou C, et al. Randomized study of individualized pharmacokinetically-guided dosing of paclitaxel compared with body-surface area dosing in Chinese patients with advanced non-small cell lung cancer. 2019;85(10):2292-301.
114. Jusko WJ. Moving from basic toward systems pharmacodynamic models. Journal of pharmaceutical sciences. 2013;102(9):2930-40.
115. Paris A, Bora P, Parolo S, Monine M, Tong X, Eraly S, et al. An age-dependent mathematical model of neurofilament trafficking in healthy conditions. CPT: pharmacometrics & systems pharmacology. 2022;11(4):447-57.

116. Paris A, Bora P, Parolo S, MacCannell D, Monine M, van der Munnik N, et al. A pediatric quantitative systems pharmacology model of neurofilament trafficking in spinal muscular atrophy treated with the antisense oligonucleotide nusinersen. CPT: pharmacometrics & systems pharmacology. 2023;12(2):196-206.
117. Carlson K, Ocean AJ. Peripheral Neuropathy with Microtubule-Targeting Agents: Occurrence and Management Approach. Clinical Breast Cancer. 2011;11(2):73-81.
118. Hertz DL, Kidwell KM, Vangipuram K, Li F, Pai MP, Burness M, et al. Paclitaxel Plasma Concentration after the First Infusion Predicts Treatment-Limiting Peripheral Neuropathy. Clinical cancer research : an official journal of the American Association for Cancer Research. 2018;24(15):3602-10.
119. Andersen NE, Boehmerle W, Huehnchen P, Stage TB. Neurofilament light chain as a biomarker of chemotherapy-induced peripheral neuropathy. Trends in Pharmacological Sciences. 2024;45(10):872-9.
120. Barroso A, Estevinho F, Hespanhol V, Teixeira E, Ramalho-Carvalho J, Araújo A. Management of infusion-related reactions in cancer therapy: strategies and challenges. ESMO Open. 2024;9(3):102922.
121. Loryan I, Fridén M, Hammarlund-Udenaes MJF, CNS Bot. The brain slice method for studying drug distribution in the CNS. 2013;10:6 -
122. Beal S SL, Boechmann A, Bauer R, editors. NONMEM 7.5 users guides. Gaithersburg, MD: ICON plc. (1989-2018).
123. Lindbom L, Pihlgren P, Jonsson EN. PsN-Toolkit--a collection of computer intensive statistical methods for non-linear mixed effect modeling using NONMEM. Computer methods and programs in biomedicine. 2005;79(3):241-57.
124. Girdenytė M, Hu Y, Ginosyan A, Hammarlund-Udenaes M, Loryan I. Formulation-dependent differences in paclitaxel distribution to anatomical sites relevant to chemotherapy-induced peripheral neuropathy. Frontiers in pharmacology. 2024;15:1486686.
125. Balayssac D, Busserolles J, Broto C, Dalbos C, Prival L, Lamoine S, et al. Neurofilament light chain in plasma as a sensitive diagnostic biomarker of peripheral neurotoxicity: In Vivo mouse studies with oxaliplatin and paclitaxel - NeuroDeRisk project. Biomedicine & pharmacotherapy = Biomedecine & pharmacotherapie. 2023;167:115535.
126. Micheli L, Balayssac D, Busserolles J, Dalbos C, Prival L, Richard D, et al. The challenge to identify sensitive safety biomarkers of peripheral neurotoxicity in the rat: a collaborative effort across industry and academia (IMI NeuroDeRisk project). Toxicology. 2024:153998.
127. Nakamura I, Ichimura E, Goda R, Hayashi H, Mashiba H, Nagai D, et al. An in vivo mechanism for the reduced peripheral neurotoxicity of NK105: a paclitaxel-incorporating polymeric micellar nanoparticle formulation. International journal of nanomedicine. 2017;12:1293-304.
128. Henningsson A SA, Loos WJ, Verweij J, Silvander M, Karlsson MO. Population Pharmacokinetic Model for Cremophor EL. PAGE. 2005;https://www.page-meeting.org/?abstract=770.
129. Kuh HJ, Jang SH, Wientjes MG, Au JL. Computational model of intracellular pharmacokinetics of paclitaxel. The Journal of pharmacology and experimental therapeutics. 2000;293(3):761-70.
130. Chen N, Brachmann C, Liu X, Pierce DW, Dey J, Kerwin WS, et al. Albumin-bound nanoparticle (nab) paclitaxel exhibits enhanced paclitaxel tissue distribution and tumor penetration. Cancer Chemother Pharmacol. 2015;76(4):699-712.

131. David-Bercholz J, Acker L, Caceres AI, Wu PY, Goenka S, Franklin NO, et al. Conserved YKL-40 changes in mice and humans after postoperative delirium. Brain, behavior, & immunity - health. 2022;26:100555.
132. Spieth L, Berghoff SA, Stumpf SK, Winchenbach J, Michaelis T, Watanabe T, et al. Anesthesia triggers drug delivery to experimental glioma in mice by hijacking caveolar transport. Neuro-oncology advances. 2021;3(1):vdab140.
133. Kuh H-J, Jang SH, Wientjes MG, Au JLS. Computational Model of Intracellular Pharmacokinetics of Paclitaxel. The Journal of pharmacology and experimental therapeutics. 2000;293(3):761-70.
134. van Zuylen L, Karlsson MO, Verweij J, Brouwer E, de Bruijn P, Nooter K, et al. Pharmacokinetic modeling of paclitaxel encapsulation in Cremophor EL micelles. Cancer Chemotherapy and Pharmacology. 2001;47(4):309-18.
135. Gornstein EL, Schwarz TL. Neurotoxic mechanisms of paclitaxel are local to the distal axon and independent of transport defects. Experimental neurology. 2017;288:153-66.
136. Koini M, Pirpamer L, Hofer E, Buchmann A, Pinter D, Ropele S, et al. Factors influencing serum neurofilament light chain levels in normal aging. 2021;13(24):25729-38.
137. Simrén J, Andreasson U, Gobom J, Suarez Calvet M, Borroni B, Gillberg C, et al. Establishment of reference values for plasma neurofilament light based on healthy individuals aged 5-90 years. Brain communications. 2022;4(4):fcac174.
138. Hossain I, Marklund N, Czeiter E, Hutchinson P, Buki A. Blood biomarkers for traumatic brain injury: A narrative review of current evidence. Brain and Spine. 2024;4:102735.
139. Samala R, Thorsheim HR, Goda S, Taskar K, Gril B, Steeg PS, et al. Vinorelbine Delivery and Efficacy in the MDA-MB-231BR Preclinical Model of Brain Metastases of Breast Cancer. Pharmaceutical Research. 2016;33(12):2904-19.
140. de Graan AJ, Lancaster CS, Obaidat A, Hagenbuch B, Elens L, Friberg LE, et al. Influence of polymorphic OATP1B-type carriers on the disposition of docetaxel. Clinical cancer research : an official journal of the American Association for Cancer Research. 2012;18(16):4433-40.
141. Nieuweboer AJ, Hu S, Gui C, Hagenbuch B, Ghobadi Moghaddam-Helmantel IM, Gibson AA, et al. Influence of drug formulation on OATP1B-mediated transport of paclitaxel. Cancer research. 2014;74(11):3137-45.
142. de Morrée ES, Böttcher R, van Soest RJ, Aghai A, de Ridder CM, Gibson AA, et al. Loss of SLCO1B3 drives taxane resistance in prostate cancer. British journal of cancer. 2016;115(6):674-81.
143. Schwaid AG, Krasowka-Zoladek A, Chi A, Cornella-Taracido I. Comparison of the Rat and Human Dorsal Root Ganglion Proteome. Scientific reports. 2018;8(1):13469.
144. Loos NHC, Martins MLF, de Jong D, Lebre MC, Tibben M, Beijnen JH, et al. Coadministration of ABCB1/P-glycoprotein inhibitor elacridar improves tissue distribution of ritonavir-boosted oral cabazitaxel in mice. International journal of pharmaceutics. 2024;650:123708.
145. van Waterschoot RA, Lagas JS, Wagenaar E, Rosing H, Beijnen JH, Schinkel AH. Individual and combined roles of CYP3A, P-glycoprotein (MDR1/ABCB1) and MRP2 (ABCC2) in the pharmacokinetics of docetaxel. Int J Cancer. 2010;127(12):2959-64.
146. Lagas JS, Damen CWN, van Waterschoot RAB, Iusuf D, Beijnen JH, Schinkel AH. P-Glycoprotein, Multidrug-Resistance Associated Protein 2, Cyp3a, and Carboxylesterase Affect the Oral Availability and Metabolism of Vinorelbine. Molecular pharmacology. 2012;82(4):636-44.

147. Taur J-S, DesJardins CS, Schuck EL, Wong YN. Interactions between the chemotherapeutic agent eribulin mesylate (E7389) and P-glycoprotein in CF-1 abcb1a-deficient mice and Caco-2 cells. Xenobiotica. 2011;41(4):320-6.
148. Torres MJ, Zhang X, Slentz DH, Koves TR, Patel H, Truskey GA, et al. Chemotherapeutic drug screening in 3D-Bioengineered human myobundles provides insight into taxane-induced myotoxicities. iScience. 2022;25(10):105189.
149. Glassman PM, Muzykantov VR. Target-mediated exposure enhancement: a previously unexplored limit of TMDD. Journal of pharmacokinetics and pharmacodynamics. 2020;47(5):411-20.
150. Loryan I, Hoppe E, Hansen K, Held F, Kless A, Linz K, et al. Quantitative Assessment of Drug Delivery to Tissues and Association with Phospholipidosis: A Case Study with Two Structurally Related Diamines in Development. Molecular Pharmaceutics. 2017;14(12):4362-73.
151. Lu H, Iuliano JN, Tonge PJ. Structure-kinetic relationships that control the residence time of drug-target complexes: insights from molecular structure and dynamics. Curr Opin Chem Biol. 2018;44:101-9.
152. Lobert S, Vulevic B, Correia JJ. Interaction of vinca alkaloids with tubulin: a comparison of vinblastine, vincristine, and vinorelbine. Biochemistry. 1996;35(21):6806-14.
153. Díaz JF, Barasoain I, Andreu JM. Fast kinetics of Taxol binding to microtubules. Effects of solution variables and microtubule-associated proteins. The Journal of biological chemistry. 2003;278(10):8407-19.

Acta Universitatis Upsaliensis

Digital Comprehensive Summaries of Uppsala Dissertations from the Faculty of Pharmacy 410

Editor: The Dean of the Faculty of Science and Technology

A doctoral dissertation from the Faculty of Science and Technology, Uppsala University, is usually a summary of a number of papers. A few copies of the complete dissertation are kept at major Swedish research libraries, while the summary alone is distributed internationally through the series Digital Comprehensive Summaries of Uppsala Dissertations from the Faculty of Science and Technology. (Prior to January, 2005, the series was published under the title “Comprehensive Summaries of Uppsala Dissertations from the Faculty of Science and Technology”.)

Distribution: publications.uu.se
urn:nbn:se:uu:diva-599159

ACTA UNIVERSITATIS
UPSALIENSIS
2026